Analysis note for transversity ITD in $a = 0.094$ fm ensemble

(Dated: June 23, 2021)

Abstract

Details of the analysis for the extraction of transversity PDF is collected together in this analysis note.

I. ENSEMBLE DETAILS

The lattice size is $32^3 \times 64$. The lattice spacing is $a = 0.094$ fm; statistics is 349; $M_\pi = 358$ MeV. The analysis is performed on ITD with momentum $P_z = 2\pi n_z/32$ with $n_z = 0, 1, 2, 3$.

II. TRANSVERSITY ITD: DEFINITIONS

The lightcone transverse ITD defined in nucleon N with spin $S = S_T$ oriented in a spatial direction $\hat{\mu} = T$ that is transverse to $\pm$- directions

$$2P_+ S_T \mathcal{M}(z_- P_+, \mu) = \langle N, S_T | \bar{\psi} \gamma_5 \gamma_+ W_+ \gamma_T | N, S_T \rangle. \tag{1}$$

The Euclidean pITD defined using nucleon moving along z-direction with its spin S in the transverse x- or y-directions is

$$2ES_T \mathcal{M}(zP_z, z^2) = \langle N; P_z, S_T | \bar{\psi} \gamma_5 \gamma_t W_z \gamma_T | N; P_z, S_T \rangle. \tag{2}$$

We will refer to the operator $\bar{\psi}\gamma_5\gamma_t\gamma_k W_z \psi$ as O_k. This is obtained from a general Lorentz decomposition for arbitrary spin S and momentum P, with $S^2 = -1, S.P = 0$, for which

$$\begin{aligned}\langle N; P, S | \bar{\psi} \gamma_5 \gamma_\mu \gamma_\nu | N; P, S \rangle = \; & 2(P_\mu S_\nu - P_\nu S_\mu) \mathcal{M}(z.P, z^2) \\ & 2im_N^2 (z_\mu S_\nu - z_\nu S_\mu) \mathcal{N}(z.P, z^2) \\ & 2m_N^2 (z_\mu P_\nu - z_\nu P_\mu) \mathcal{R}(z.P, z^2).\end{aligned} \tag{3}$$

III. CONSTRUCTING THE CORRELATORS FROM REDSTAR HELICITY BASIS

We will be extracting the required positive parity ground state matrix element from the 3pt function,

$$C_{3\text{pt}}(t_s,\tau) = \left\langle [\bar{N}^+]^\alpha (1+\gamma_5\gamma_k)^{\alpha\beta} O_k [N^+]^\beta \right\rangle , \tag{4}$$

where $N^+ = (1+\gamma_t)N$. The gamma matrix basis that is used is the Pauli-Dirac representation:

$$\gamma_t = \begin{pmatrix} 1 & 0 \\ 0 & -1 \end{pmatrix} ; \gamma_k = \begin{pmatrix} 0 & \sigma_k \\ -\sigma_k & 0 \end{pmatrix} ; \gamma_5 = \begin{pmatrix} 0 & 1 \\ 1 & 0 \end{pmatrix} . \tag{5}$$

In this basis, the spin projection operator acting on upper two components, $[N^+]^\alpha$, for spin S in the k-th direction $\mathcal{P}_{k\pm} = (1 \pm \gamma_5 \not{S}) = (1 \pm \gamma_5\gamma_k)$ becomes

$$\mathcal{P}_{k\pm} = (1 \pm \sigma_k). \tag{6}$$

Writing

$$N^+ = \begin{pmatrix} N_{z+} \\ N_{z-} \end{pmatrix} . \tag{7}$$

Here $(N_{z+}, 0)$ and $(0, N_{z-})$ are the ± 1 eigenstates of $\mathcal{P}_{z\pm}$ respectively. In this convention, the correlator we want is

$$C_{3\text{pt}}^{k+,k+} = \left\langle N^+ \mathcal{P}_{k+} O_k \mathcal{P}_{k+} N^+ \right\rangle . \tag{8}$$

What is being stored in redstar at are the correlators

$$C_{3\text{pt}}^{\pm,\pm} = \begin{cases} \langle N^+ \mathcal{P}_{z\pm} O_k \mathcal{P}_{z\pm} N^+ \rangle & \text{for} \quad P_z = 0 \\ \langle N^+ \mathcal{P}_{x\pm} O_k \mathcal{P}_{x\pm} N^+ \rangle & \text{for} \quad P_z \neq 0 \end{cases} . \tag{9}$$

The $\pm$ indices are the "rows" in the redstar files. We should linearly combine the above components being stored in the data to get correlator we want. For $P_z = 0$, we can construct

$$\begin{aligned} C^{x+,x+} &= C^{z+,z+} + C^{z+,z-} + C^{z-,z+} + C^{z-,z-}, \\ C^{y+,y+} &= C^{z+,z+} + iC^{z+,z-} - iC^{z-,z+} + C^{z-,z-}, \\ C^{z+,z+} &= C^{z+,z+}. \end{aligned} \tag{10}$$

For $P_z \neq 0$, the useful combinations are

$$\begin{aligned} C^{x+,x+} &= C^{x+,x+}, \\ C^{y+,y+} &= C^{x+,x+} - iC^{x+,x-} + iC^{x-,x+} + C^{x-,x-}, \\ C^{z+,z+} &= C^{x+,x+} + C^{x+,x-} + C^{x-,x+} + C^{x-,x-}. \end{aligned} \tag{11}$$

IV. MATCHING

The matching kernel for transversity ratio ITD is [Morris, Radyushkin in prep]:

$$\mathcal{M}(\nu, z^2) = \int_0^1 du C(u, \mu^2 z^2) I(u\nu, \mu), \tag{12}$$

with

$$C(u, \mu^2 z^2) = \delta(1-u) - \frac{\alpha_s C_F}{2\pi} \left\{ \left[\frac{2u}{1-u}\right]_+ \log\left(z^2\mu^2 e^{2\gamma_E+1}/4\right) + 4\left[\frac{\log(1-u)}{1-u}\right]_+ \right\}. \tag{13}$$

The normalization is such that $\langle x^0 \rangle = 1$. For convenience in numerical implementation, we rewrite the relation as

$$\mathcal{M}(\nu, z^2) = 1 + \sum_{n=1} \langle x^n \rangle(\mu) c_n(z^2\mu^2) \frac{(-i\nu)^n}{n!}. \tag{14}$$

The coefficients c_n are the Mellin moments of $C(u, \mu^2 z^2)$, given by

$$\begin{aligned} c_n(z^2\mu^2) &= \int_0^1 C(u, \mu^2 z^2) u^n du, \\ &= 1 - \frac{\alpha_s C_F}{2\pi} \left\{ 2(1 - H_{n+1}) \log\left(z^2\mu^2 e^{2\gamma_E+1}/4\right) + \frac{1}{3}\left(\pi^2 + 6H_n^2 - 6\psi^{(1)}(1+n)\right) \right\}. \end{aligned} \tag{15}$$

V. EXTRACTION OF MATRIX ELEMENTS BY TWO-STATE FITS AND SUMMATION METHOD

We analyze the 2-pt function by fits to the spectral decomposition,

$$C_{\mathrm{2pt}}(t_s) = \sum_{i=0}^{N-1} A_i e^{-E_i t_s}. \tag{16}$$

We will use 1-state fits over ranges $t_s \in [t_{\min}, 18a]$ with $t_{\min} > 8a$, and 2-state fits over ranges $t_s \in [t_{\min}, 18a]$ for $t_{\min} = 2, 3, 4$ respectively. With this, we obtain a jack-knife sample of fits parameters A_i, E_i, which we input into the analysis of 3pt functions.

For the 3pt functions, we first form the ratio,

$$R(t_s, \tau) \equiv \frac{C_{\mathrm{3pt}}(t_s, \tau)}{C_{\mathrm{2pt}}(t_s)}, \tag{17}$$

at different z and P_z. Two kinds of analysis is performed. In the fitting method, we fit the spectral decomposition,

$$R(t_s, \tau) = \frac{\sum_{i,j=0}^{N-1} M_{ij} A_i A_j^* e^{-E_i(t_s-\tau)+E_j\tau}}{\sum_{i}^{N-1} A_i^2 e^{-E_i t_s}}. \tag{18}$$

over the data spanning the range of $t_s \in [t_{\min}, t_{\max}]$ and $\tau \in [\tau_0, t_s - \tau_0]$. We denote this fit as $\mathrm{Fit}(N, t_{\min}, t_{\max}, \tau_0)$. The fit parameters are M_{ij}. In this note, we will restrict ourself to $\mathrm{Fit}(2, t_{\min}, 18, 2)$, with $t_{\min} = 6, 8$.

In the summation method, we will compute

$$S(t_s, \tau_0) = \sum_{\tau=\tau_0}^{t_s-\tau_0} R(t_s, \tau). \tag{19}$$

In the fit of type $\mathrm{Sum}(t_{\min}, t_{\max}, \tau_0)$, we will fit S to straight line,

$$S(t_s; \tau_0) = M_{00} + c t_s, \tag{20}$$

over the data in $t_s \in [t_{\min}, t_{\max}]$. In the plots shown, we will use Sum(6,18,2) and Sum(8,18,2).

To estimate the ground state M.E. M_{00}, we average over the results from the 2-state fit extrapolation and the result from summation fit. This M_{00} is the bare ITD using O_k operator (which uses $\gamma_5\gamma_t\gamma_k$ gamma structure), and will we call it $\mathcal{M}_k^B(z, P_z)$.

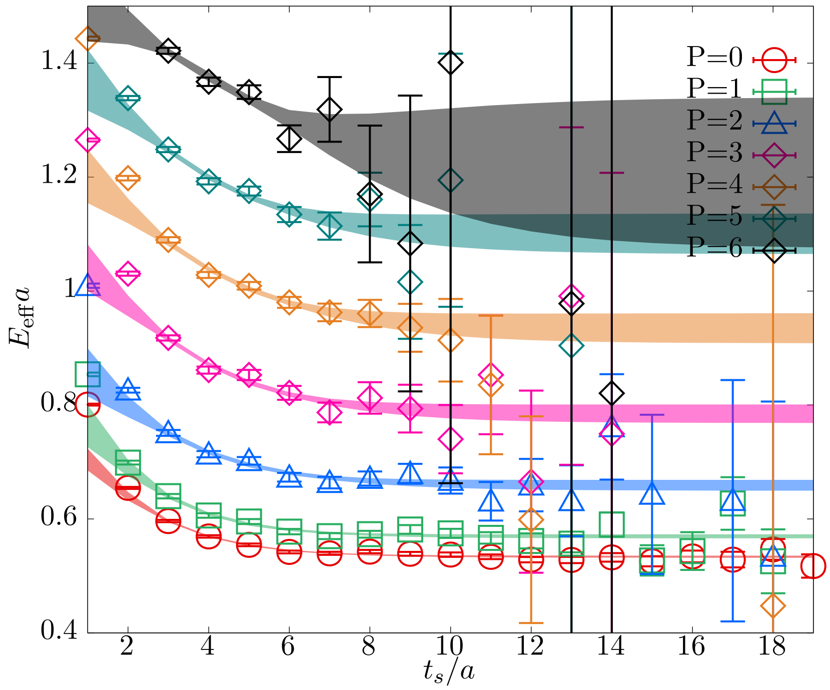

FIG. 1. The effective mass at different P_z are shown in different colors. The bands are the expected t_s dependence of E_{eff} from two-state fit over $t_s \in [3a, 18a]$.

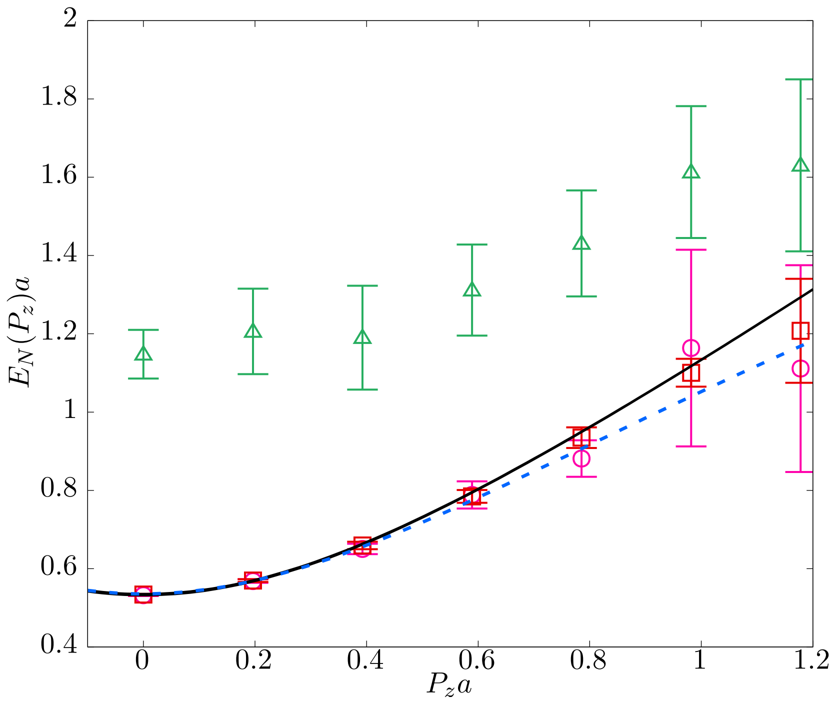

FIG. 2. The dispersion relation for ground state and 1st excited state from 2-state fits are shown. For the ground state, the energies from the 2-state ($t_s \in [3a, 18a]$) and 1-state ($t_s \in [10a, 18a]$) are shown. The solid curve is continuum single particle dispersion and the dashed curve is the lattice single particle dispersion. These values of E_i will be used in the extrapolation of 3-pt functions.

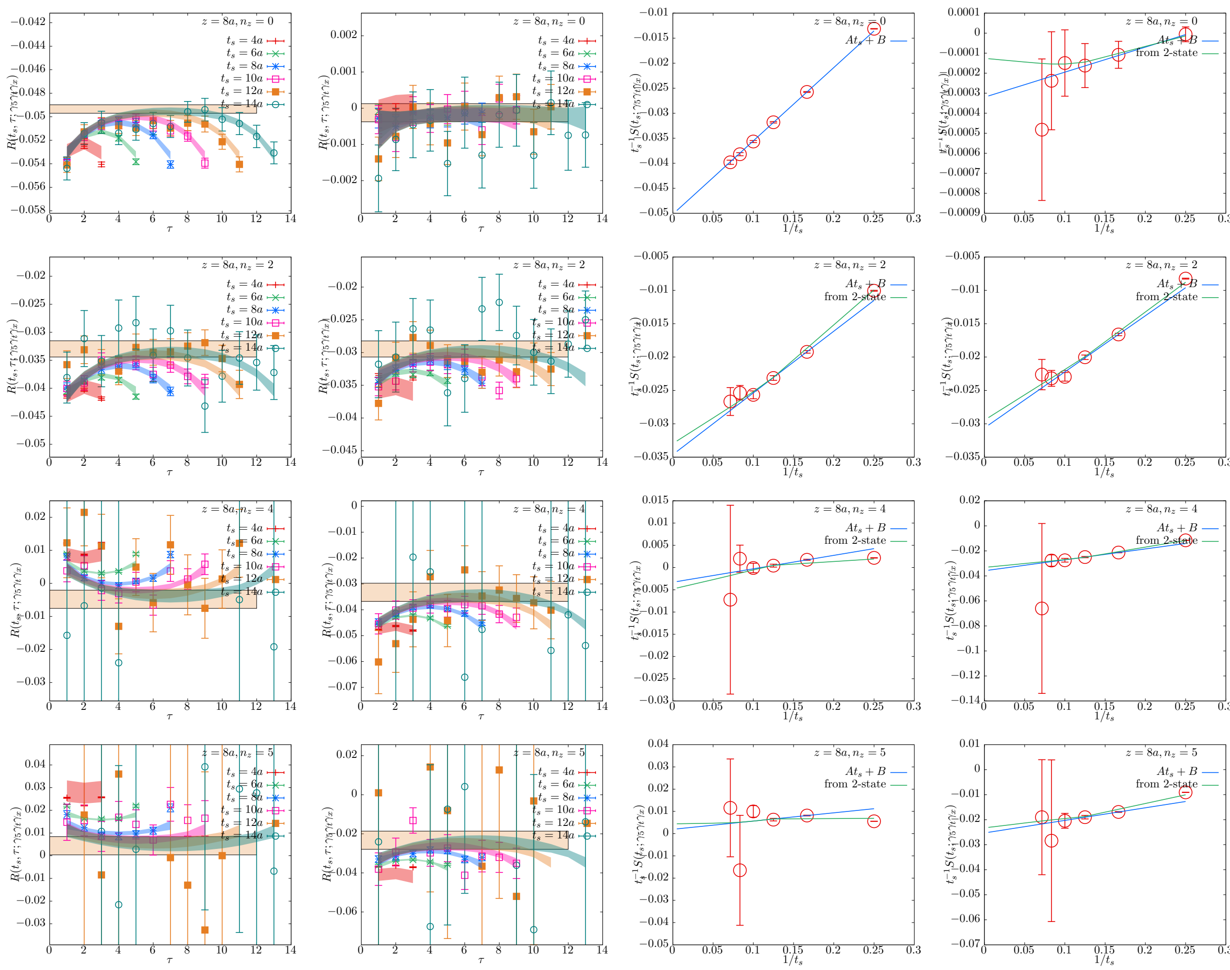

FIG. 3. Determination of ground state bare matrix element at a sample point $z = 8a$ at different set of momenta, $n_z = 0, 2, 4, 5$ in the four rows respectively. The first two panels show the 2-state extrapolation of real and imaginary parts from the 3pt to 2pt ratio R. The third and the fourth panels show the fits from the summation method for the real and imaginary parts respectively.

VI. RENORMALIZATION

We renormalize via the RGI ratios. However, there are some choice here:

Choice-1 is to treat x and y directions independently:

$$\mathcal{M}_k(zP_z, z^2) \equiv \frac{\mathcal{M}_k^B(z, P_z)}{\mathcal{M}_k(z, 0)}. \tag{21}$$

Choice-2 making the rotational invariance to be exact:

$$\mathcal{M}(zP_z, z^2) \equiv \frac{\mathcal{M}_x^B(z, P_z) + \mathcal{M}_y^B(z, P_z)}{\mathcal{M}_x(z, 0) + \mathcal{M}_y(z, 0)}. \tag{22}$$

We will make use of Choice-2 in order to explicitly impose all the expected symmetries.

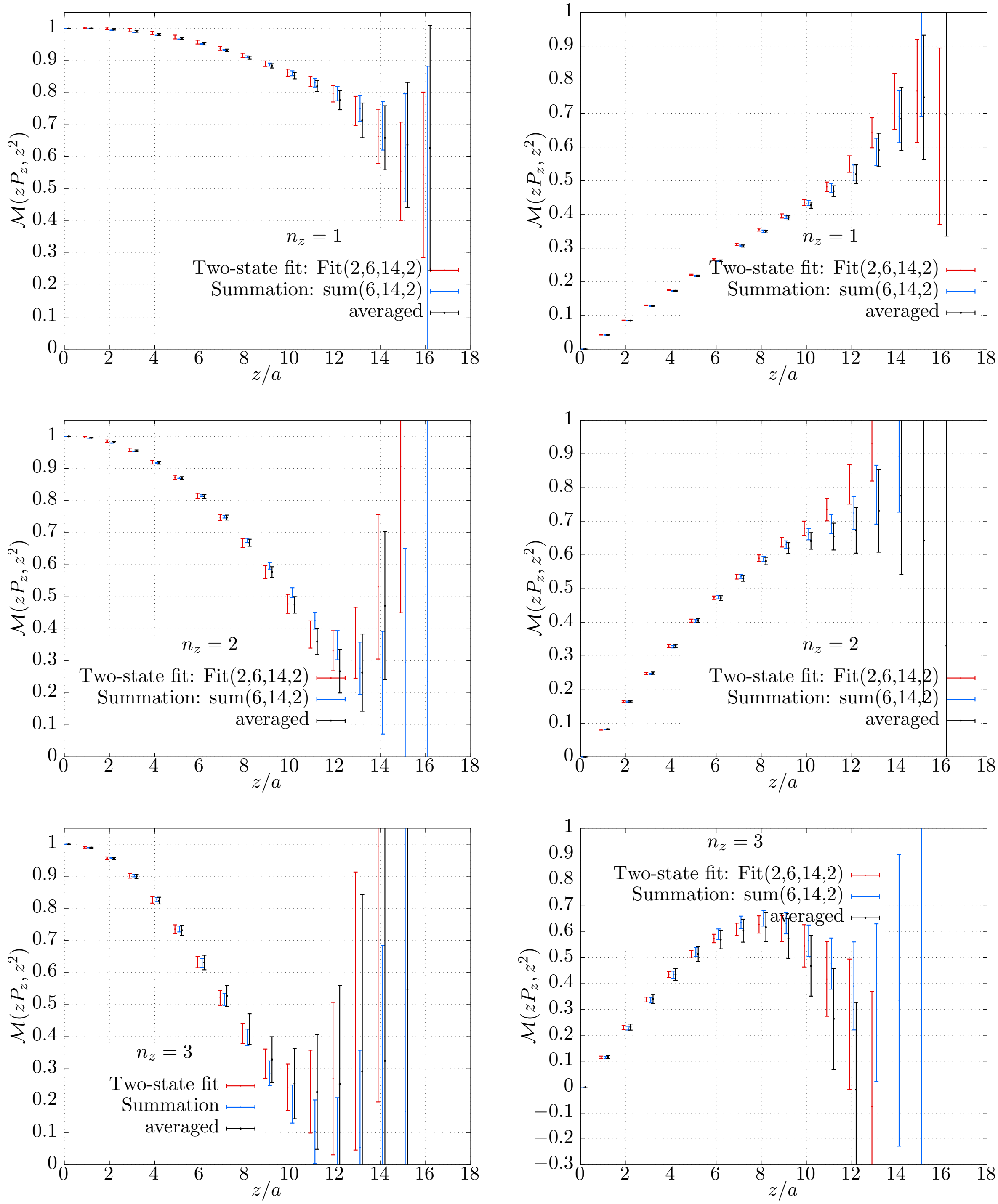

FIG. 4. The real (left) and imaginary (right) parts of the renormalized matrix elements using two-state fit (red), summation fit (blue) and their average (black) at momenta $n_z = 1, 2, 3$.

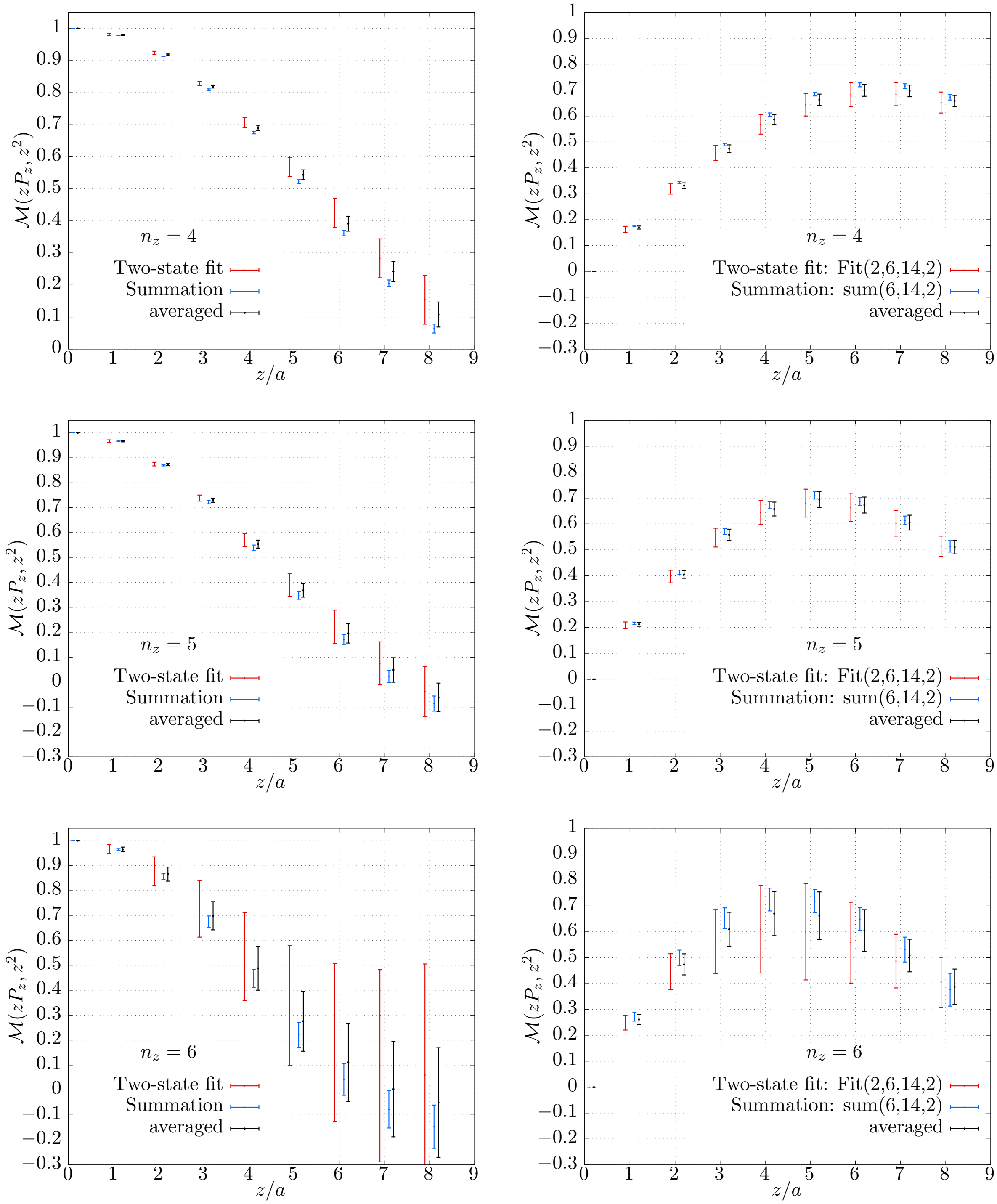

FIG. 5. The real (left) and imaginary (right) parts of the renormalized matrix elements using two-state fit (red), summation fit (blue) and their average (black) at momenta $n_z = 4, 5, 6$.

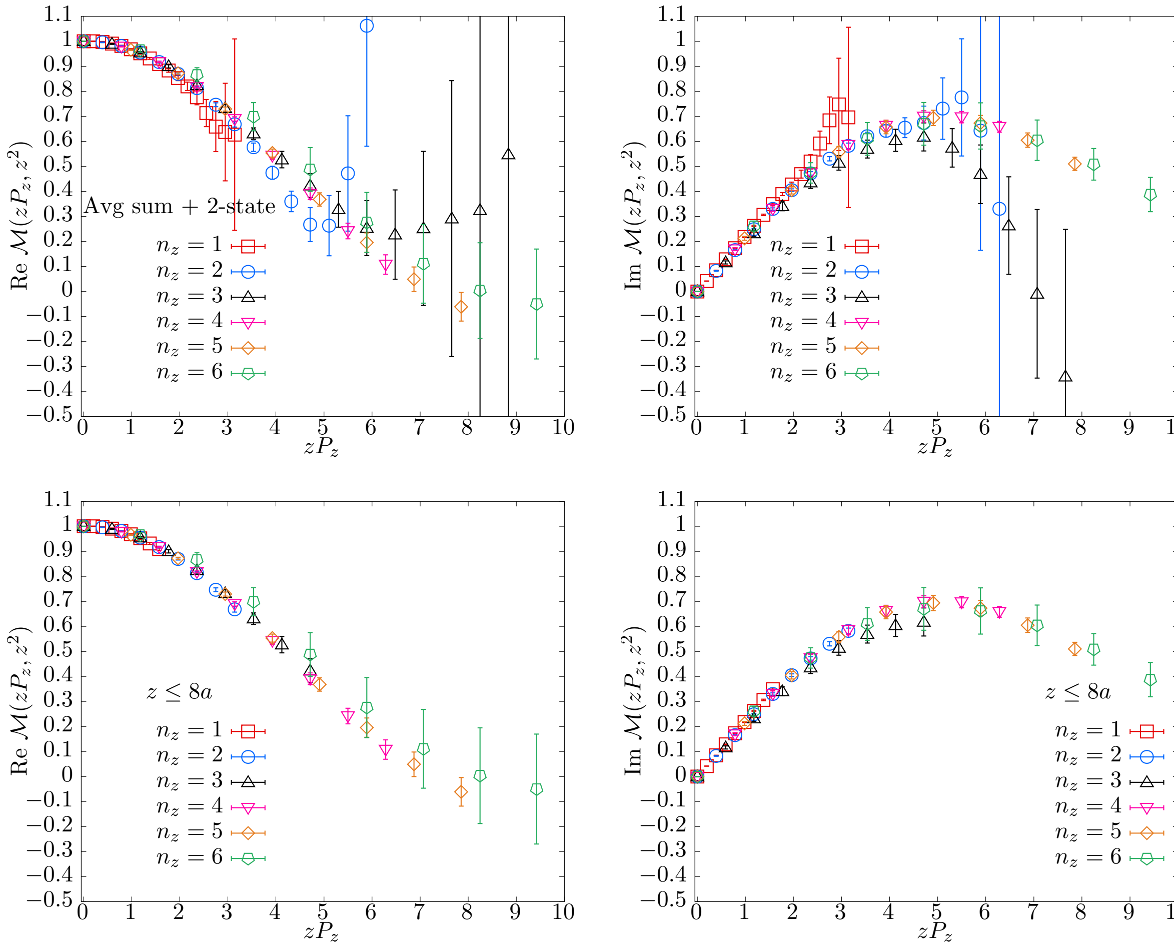

FIG. 6. The ITD is shown by putting together the data from all momenta differentiated by the colors. In the top panel, the data with all available z are shown. In the bottom panel, only the data with $z \leq 8a = 0.77$ fm are shown.

VII. EVIDENCES FOR THE SHORT-DISTANCE LATTICE CORRECTIONS

We look for the lattice corrections present in the lattice data by performing the OPE w/o OPE analysis by fitting the data as a function of ν at different fixed z. From this we extract the moments $\langle x^n \rangle$, with the number of moments in the OPE as $N_{\rm max} = 2, 4, 6$. By looking at the z dependence of $\langle x^n \rangle$ we find evidences for the type of correction present to the continuum twist-2 OPE. From Fig. 7, we find that the imaginary part suffers from $a\nu/z$ lattice correction, whereas there is no signal for any lattice correction present in the real part. For $\langle x^3 \rangle$, the data is noisy enough that there is again no evidence for a $a\nu^3/z$ type correction is seen. Therefore we will include a minimal correction of the form $a\nu/z$ to both the real and imaginary parts of the OPE.

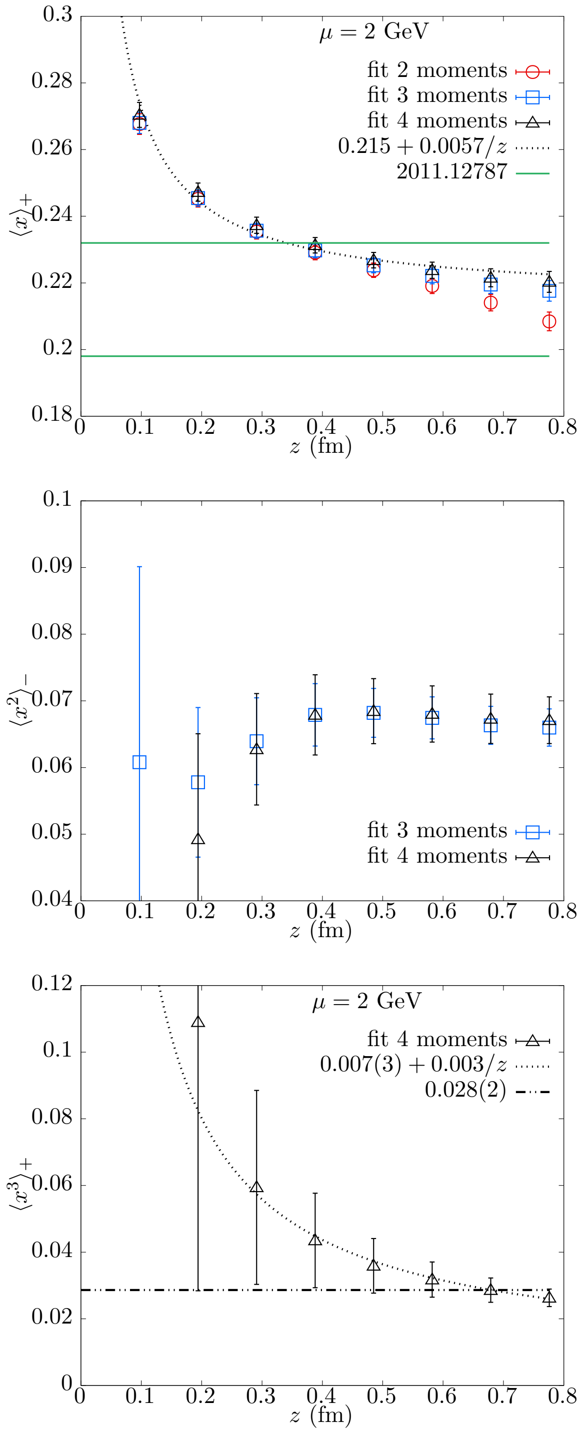

FIG. 7. The top panel shows the z-dependence of the $\langle x \rangle$ moment extracted as a function of z by including 2,4,6 moments in the twist-2 OPE. The dashed line is the fit with $\langle x \rangle + a/z$ which translates to the presence of $a\nu/z$ type lattice correction. For comparison, the value of $\langle x \rangle$ from 2011.12787 is shown as the green band. The middle and the bottom panels show similar results for $\langle x^2 \rangle$ and $\langle x^3 \rangle$ respectively.

VIII. ANALYSIS BY FITTING MOMENTS AS FREE PARAMETERS

In this analysis, we fit the data to

$$\mathrm{Re}\mathcal{M}(\nu, z^2) = 1 + \left(\sum_{n=2,4,\ldots}^{N_{\max}} C_n(\mu^2 z^2)\langle x^n\rangle_- \frac{(-i\nu)^n}{n!}\right) + \frac{d_r a}{z}\nu^2 + b_r z^2 \nu^2,$$
$$\mathrm{Im}\mathcal{M}(\nu, z^2) = 1 + \left(\sum_{n=1,3,\ldots}^{N_{\max}} C_n(\mu^2 z^2)\langle x^n\rangle_+ \frac{(-i\nu)^n}{n!}\right) + \frac{d_i}{z}\nu + b_i z^2 \nu. \tag{23}$$

We fit up to 4 moments as free parameters each for real and imaginary parts in the analysis where moments are free parameter. Later on, when we use fit ansatz, we will use up to 30 moments.

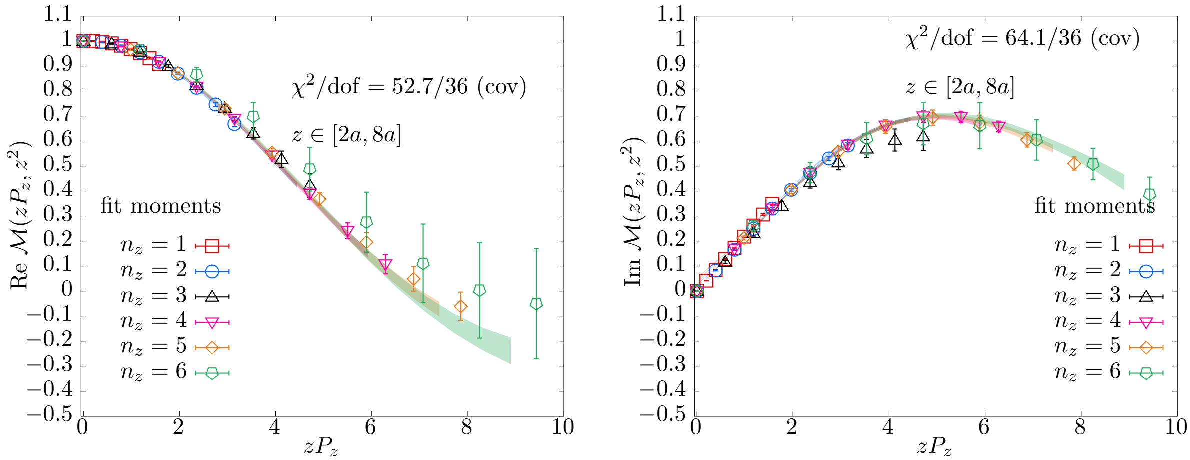

FIG. 8. Fit to real and imaginary parts of the ITD based on fits to the moments.

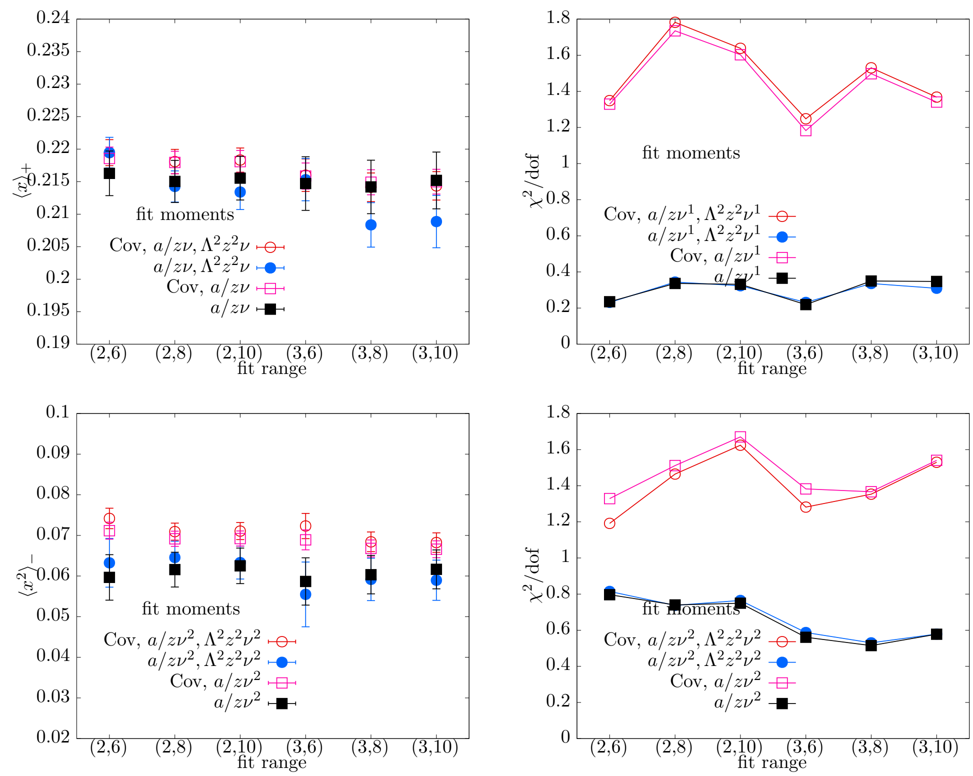

FIG. 9. The top-left panel shows $\langle x \rangle_+$ obtained from fits whose fit ranges (x-axis) and model for lattice corrections and higher=twist corrections are shown. The fits were performed with and without covariance matrices. The top-right panel shows the χ^2/dof for all these fits. The bottom panels show similar plots for $\langle x^2 \rangle_-$ and the χ^2/dof for the fits to the real part of the ITD.

IX. ANALYSIS BY FITS USING THE 2-PARAMETER ANSATZ $x^\alpha(1-x)^\beta$

We first fit the data by using the PDF Ansatze,

$$f_\pm = \mathcal{N}_\pm x^{\alpha_\pm}(1-x)^{\beta_\pm}. \tag{24}$$

The values of $(\alpha_\pm, \beta_\pm)$ will be used as priors in the 4-parameter analysis.

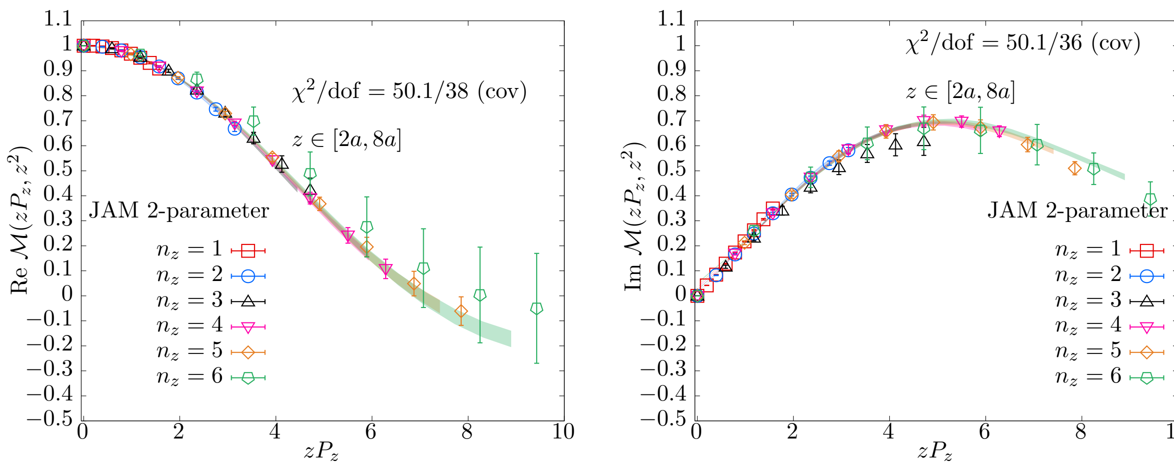

FIG. 10. Fits using two-parameter JAM ansatz. The data points are the rITD at various fixed P_z. Only $z < 0.77$ fm are shown and used for the analysis shown (shorter $z_{\max}$ shown later). The real and imaginary parts are in the left and right panels. The bands are the fits to moments.

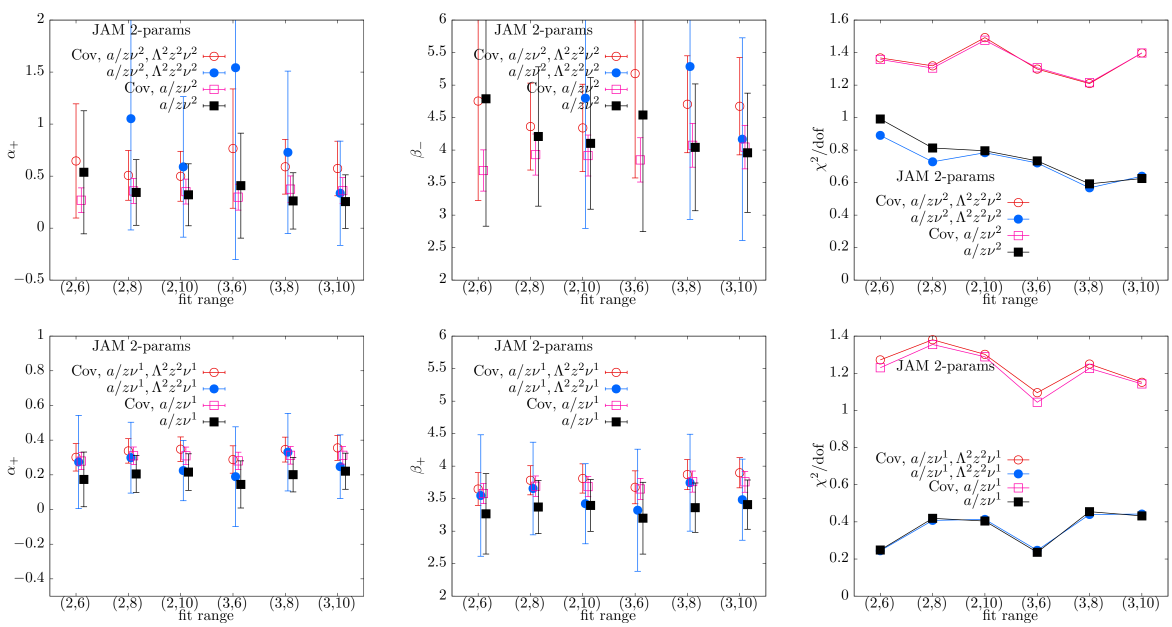

FIG. 11. The top panels show $\alpha_-, \beta_-, \chi^2/\mathrm{dof}$ obtained from 2-parameter JAM fits to real-part of ITD are shown. The bottom panels show $\alpha_+, \beta_+, \chi^2/\mathrm{dof}$ obtained from 2-parameter JAM fits to imaginary-part of ITD are shown.

X. ANALYSIS BY FITS USING THE 4-PARAMETER ANSATZ

We fit the ITD data by using the PDF Ansatze,

$$f_{\pm} = \mathcal{N}_{\pm} x^{\alpha_{\pm}} (1-x)^{\beta_{\pm}} (1 + \gamma_{\pm}\sqrt{x} + \delta_{\pm} x). \tag{25}$$

The fits were made using priors on $(\alpha_{\pm}, \beta_{\pm})$ with the central-values of priors taken from the corresponding 2-parameter fits with the same fit-ranges, and the prior-widths equal to their 1-σ statistical error in 2-parameter fits.

In doing such fits, $f_{\pm}(x)$ was decomposed into their Jacobi polynomial basis $P_n^{\alpha_{\pm},\beta_{\pm}}(1-2x)$. Through this, the means and errors on Jacobi basis components were obtained.

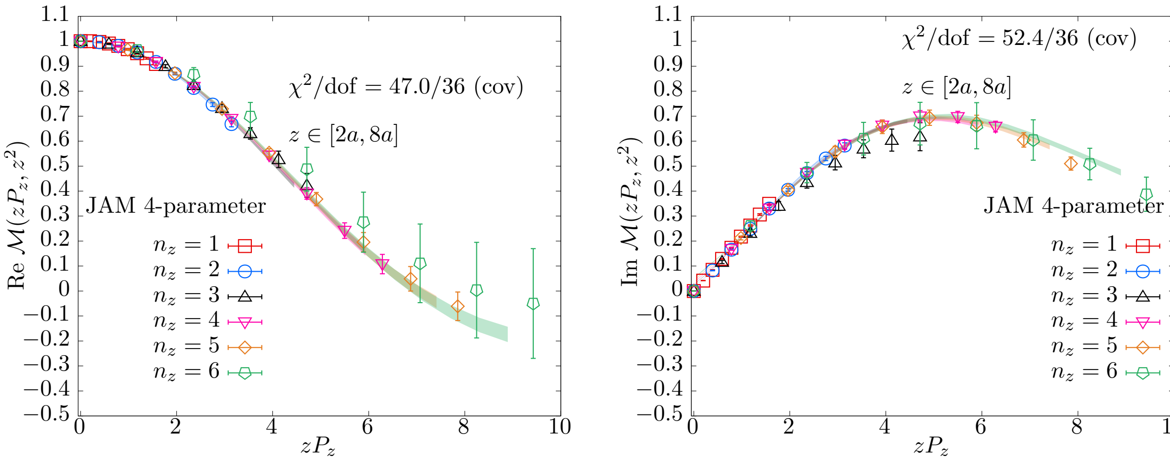

FIG. 12. Fits using four-parameter JAM ansatz. The data points are the rITD at various fixed P_z. Only $z < 0.77$ fm are shown and used for the analysis shown (shorter $z_{\max}$ shown later). The real and imaginary parts are in the left and right panels. The bands are the fits to moments.

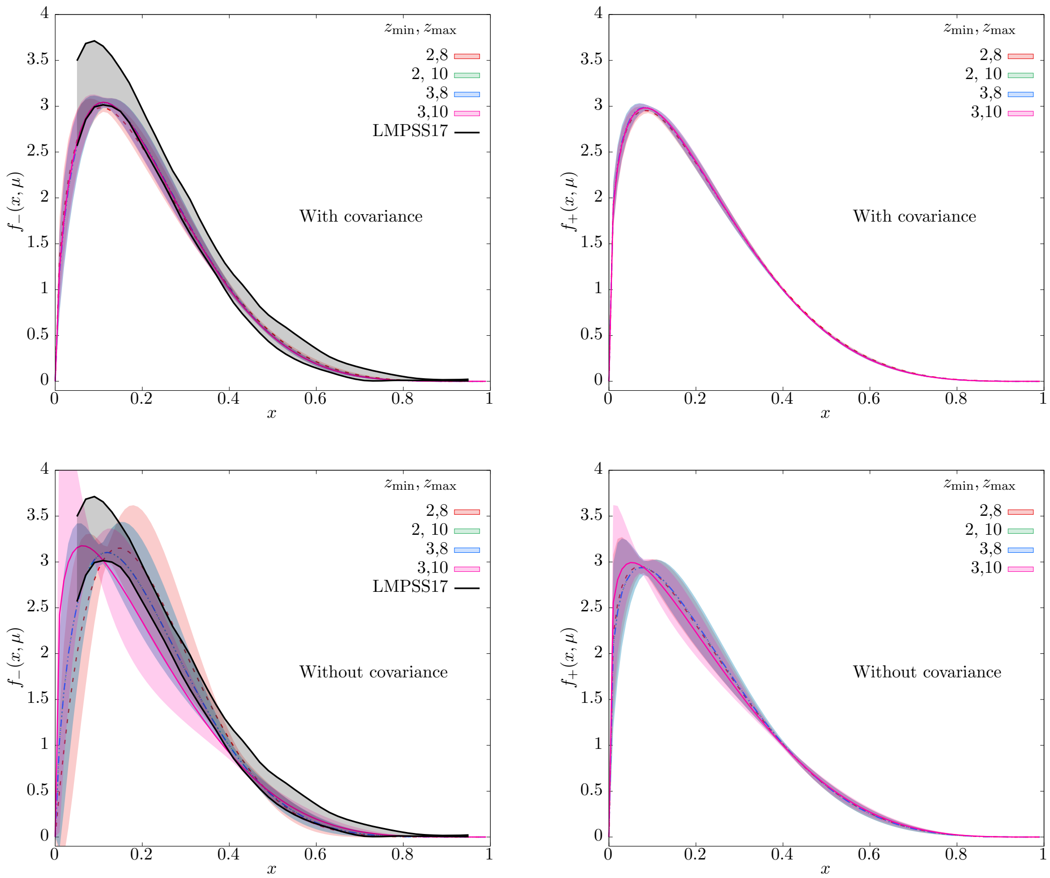

FIG. 13. The top two panels show $f_-(x)$ reconstructed based on 4-parameter ansatz. The top-left panel made of covariance matrix in the fits, and the top-right panel did not use it. In each of the panels, the different colored bands show variations coming from changes in fit ranges in $z \in [z_{\min}, z_{\max}]$. For $f_-(x)$, the result from (global fit+lattice g_T) from arXiv:1710.09858 are shown by the black band, such that the area within the black band is 1. Similar plots are for $f_+(x)$ are shown in the bottom panels.

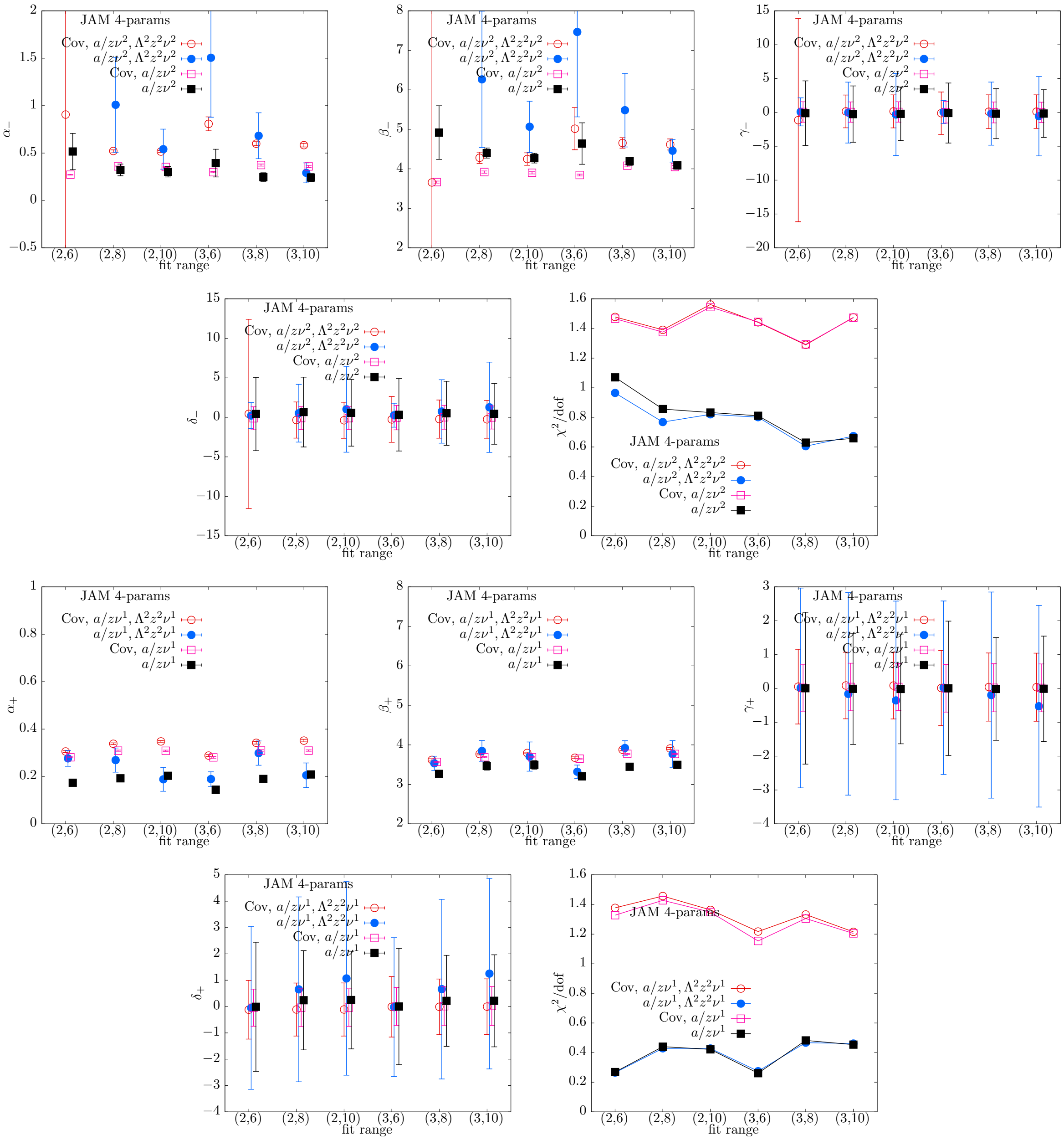

FIG. 14. The top set of panels show $\alpha_-, \beta_-, \gamma_-, \delta_-, \chi^2$/dof obtained from 4-parameter JAM fits to real-part of ITD are shown. The values of α_-, β_- were constrained by priors, and no priors on γ_-, δ_-. The bottom set of panels show $\alpha_+, \beta_+, \gamma_+, \delta_+, \chi^2$/dof obtained from 4-parameter JAM fits to imaginary-part of ITD are shown. The values of α_+, β_+ were constrained by priors, and no priors on γ_+, δ_+.

XI. FITS TO PDF USING JACOBI FUNCTIONS.

Refer to arxiv:2105.13313 for a complete description. The key points are

- The PDF is written as

$$f_{\pm}(x) = x^{\alpha_{\pm}}(1-x)^{\beta_{\pm}} \sum_{n}^{N_{\max}} s_n^{\pm} P_n^{\alpha,\beta}(1-2x). \tag{26}$$

  The choice of $\alpha_{\pm}$ and $\beta_{\pm}$ are arbitrary. If $N_{\max} = \infty$, then it is exact. However, we need to truncate $N_{\max}$ to $O(1)$.

- $\int_0^1 x^{\alpha}(1-x)^{\beta} P_n^{\alpha,\beta}(1-2x) P_m^{\alpha,\beta}(1-2x) dx \propto \delta_{n,m}$.

- With this, we can fit the ITD to

$$\begin{aligned}
\mathcal{M}(\nu, z^2) &= \sum_{n=0}^{N_{\max}} s_n G_n(z^2, \nu; \alpha, \beta), \\
G_n(z^2, \nu; \alpha, \beta) &= \sum_{k=1}^{\infty} \frac{(-i\nu)^k}{k!} c_k(\mu^2 z^2) \int_0^1 dx x^{\alpha}(1-x)^{\beta} x^k P_n^{\alpha,\beta}(1-2x).
\end{aligned} \tag{27}$$

XII. METHOD FOR THE JACOBI FITS

We chose a fixed α, β for the Jacobi basis from the central values of $\alpha_{\pm}, \beta_{\pm}$ from the corresponding 4-parameter JAM fits. For the Jacobi polynomial components, we imposed a prior equal to $3 \times \sigma_{\text{stat}}$ of the components obtained by decomposing the 4-parameter JAM fits. Then we varied the number of components to look for stability.

XIII. QUANTIFYING PERTURBATIVE UNCERTAINTY

In addition to fixing the value of $\alpha_s(\mu)$ at fixed value, we also performed an analysis where we introduced a Gaussian noise in $\alpha_s(\mu)$ with 20% error. That is $\alpha_s \sim \mathcal{N}(\bar{\alpha}_s, 0.2\bar{\alpha}_s)$.

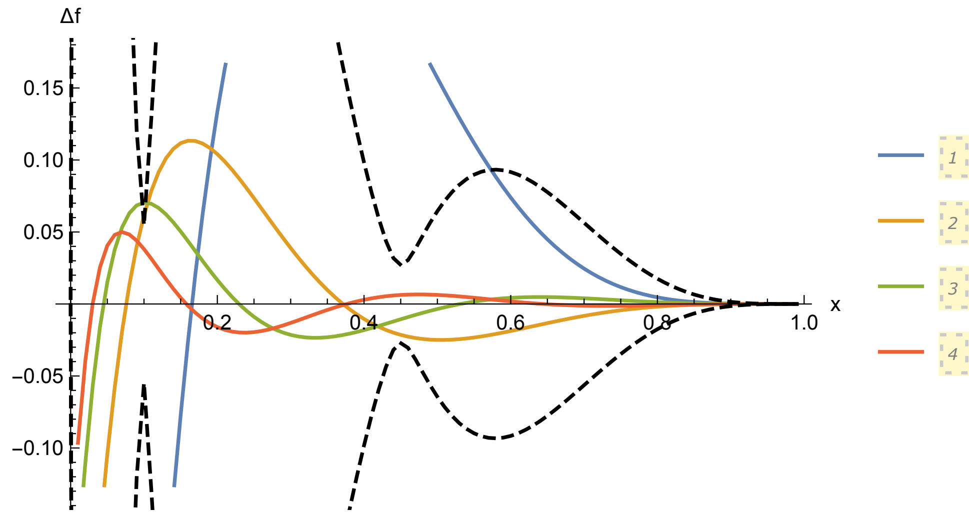

FIG. 15. Rationale for the convergence of Jacobi polynomial fits for functions that resemble typical PDFs. From the 3-parameter JAM type fit to the real part, we found $f(x) \sim x^{0.3(6)}(1-x)^{4.5(1.8)}(1+3.1(4)\sqrt{x})$. Here, we expand this function in terms of Jacobi polynomial in Eq. (26) with same α and β from $f(x)$, and ask how it converges as a function of truncation value of $N_{\max}$. The plot shows the "error" which is the difference between f(x) and Jacobi polymial expansion of f(x) upto $N_{\max}$, for different $N_{\max}$. To compare, the error band in $f(x)$ itself is enclosed between the dashed black lines. It shows $N_{\max} = 2$ or 3 is sufficient for $\alpha \approx 0.3$ and $\beta \approx 4$.

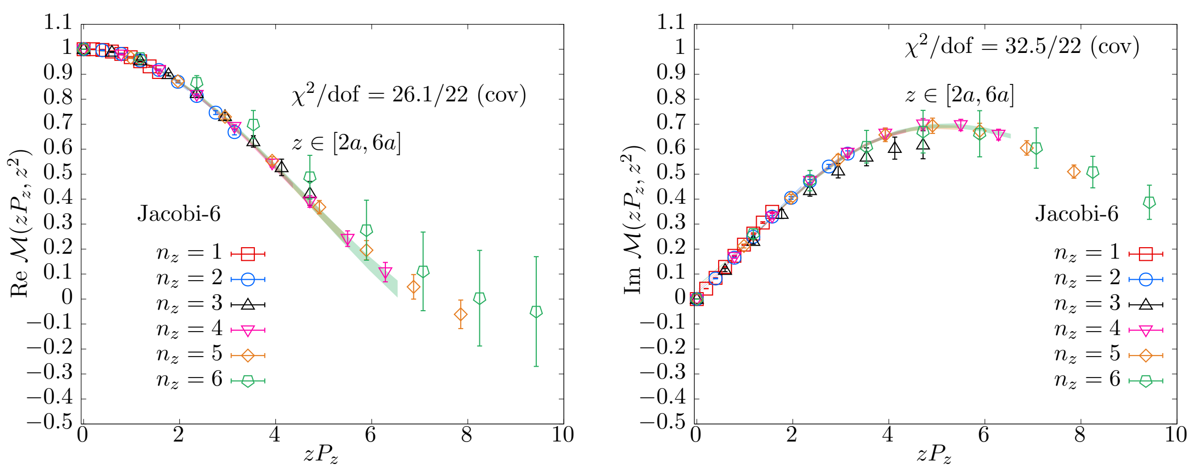

FIG. 16. Fits using Jacobi polynomials upto order 6. The data points are the rITD at various fixed P_z. Only $z < 0.77$ fm are shown and used for the analysis shown (shorter $z_{\max}$ shown later). The real and imaginary parts are in the left and right panels. The bands are the fits to moments.

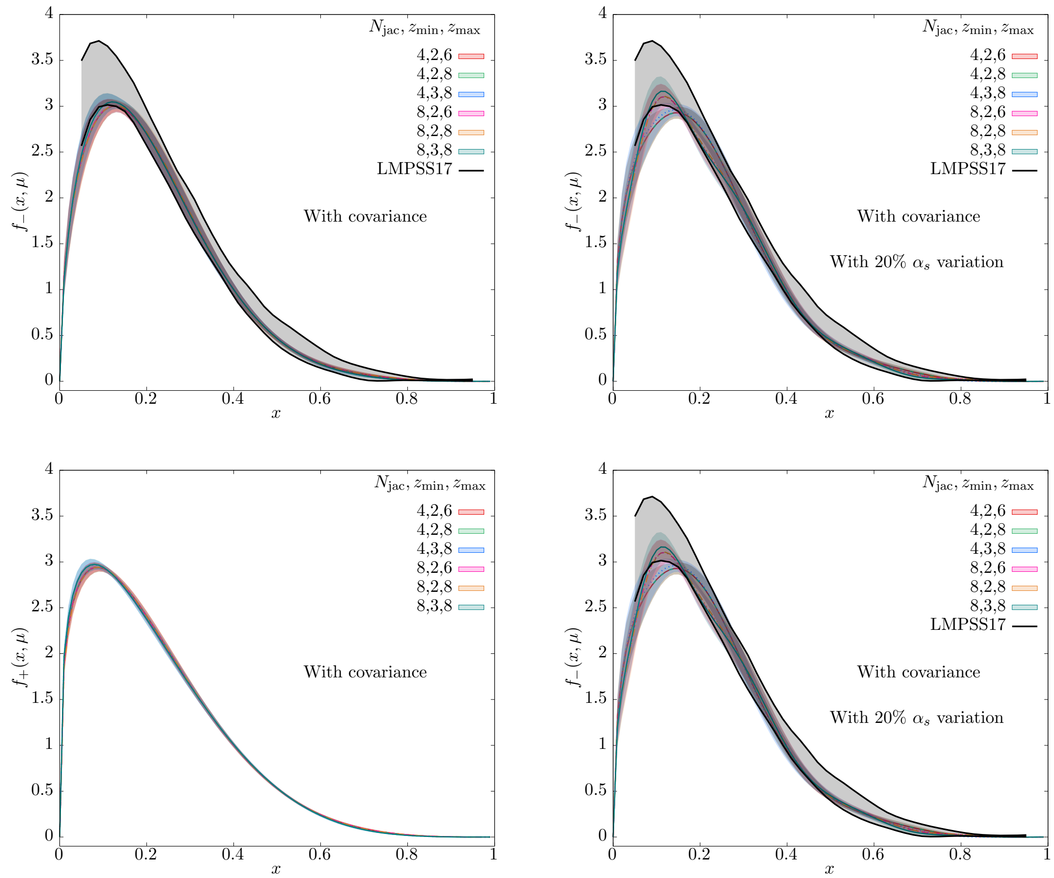

FIG. 17. (PDF from fits with covariance matrix) The top two panels show $f_-(x)$ reconstructed based on 4-parameter ansatz. A fixed value of $\alpha_s = 0.3$ was for matching in the top-left panel, whereas $\alpha_s \in \mathcal{N}(0.3, 0.06)$ in the top-right panel. In each of the panels, the different colored bands show variations coming from using order $N_{\rm jac} = 4, 8$ Jacobi basis and due to the changes in fit ranges in $z \in [z_{\rm min}, z_{\rm max}]$. For $f_-(x)$, the result from (global fit+lattice g_T) from arXiv:1710.09858 are shown by the black band, such that the area within the black band is 1. Similar plots are for $f_+(x)$ are shown in the bottom panels.

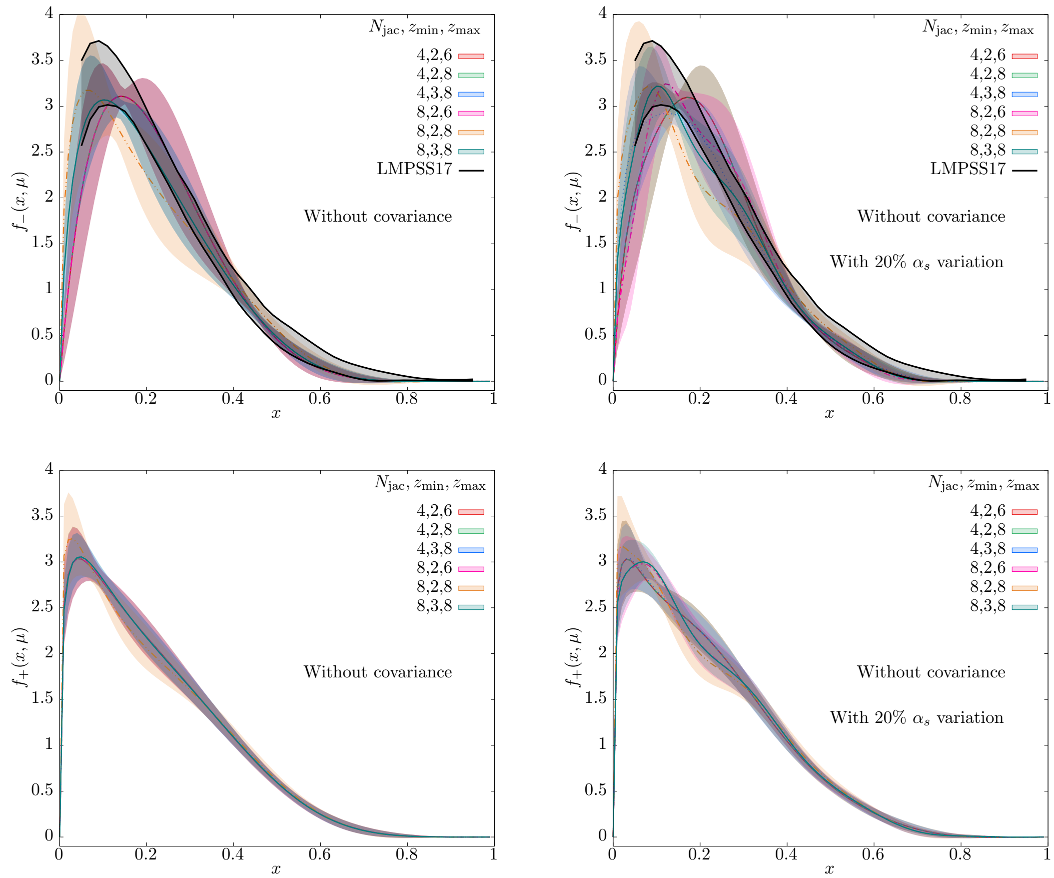

FIG. 18. (PDF from fits without covariance matrix) The top two panels show $f_-(x)$ reconstructed based on 4-parameter ansatz. A fixed value of $\alpha_s = 0.3$ was for matching in the top-left panel, whereas $\alpha_s \in \mathcal{N}(0.3, 0.06)$ in the top-right panel. In each of the panels, the different colored bands show variations coming from using order $N_{\rm jac} = 4, 8$ Jacobi basis and due to the changes in fit ranges in $z \in [z_{\rm min}, z_{\rm max}]$. For $f_-(x)$, the result from (global fit+lattice g_T) from arXiv:1710.09858 are shown by the black band, such that the area within the black band is 1. Similar plots are for $f_+(x)$ are shown in the bottom panels.

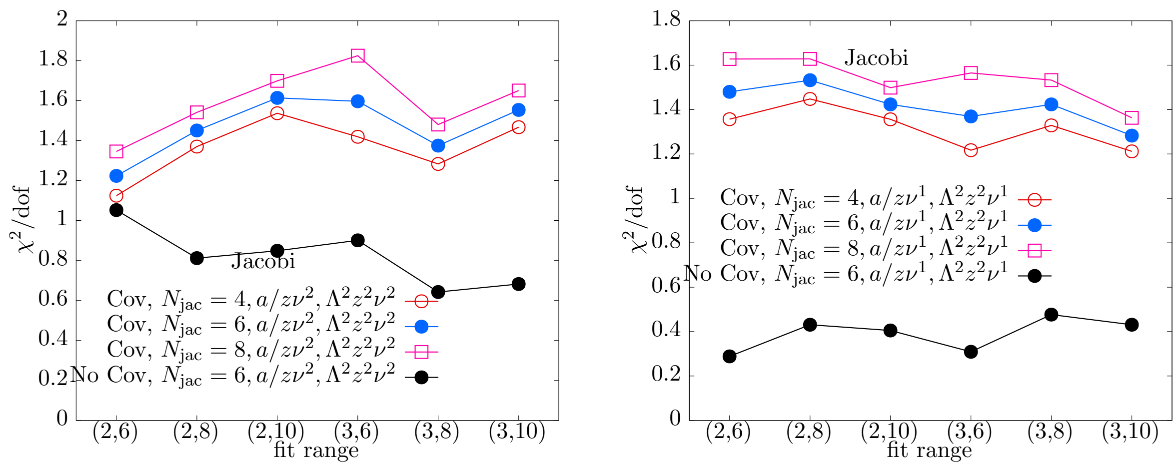

FIG. 19. χ^2/dof from the fits to the real (left) and imaginary (right) parts. The variations from fit ranges and choice of lattice correction and number of Jacobi polynomials are shown.

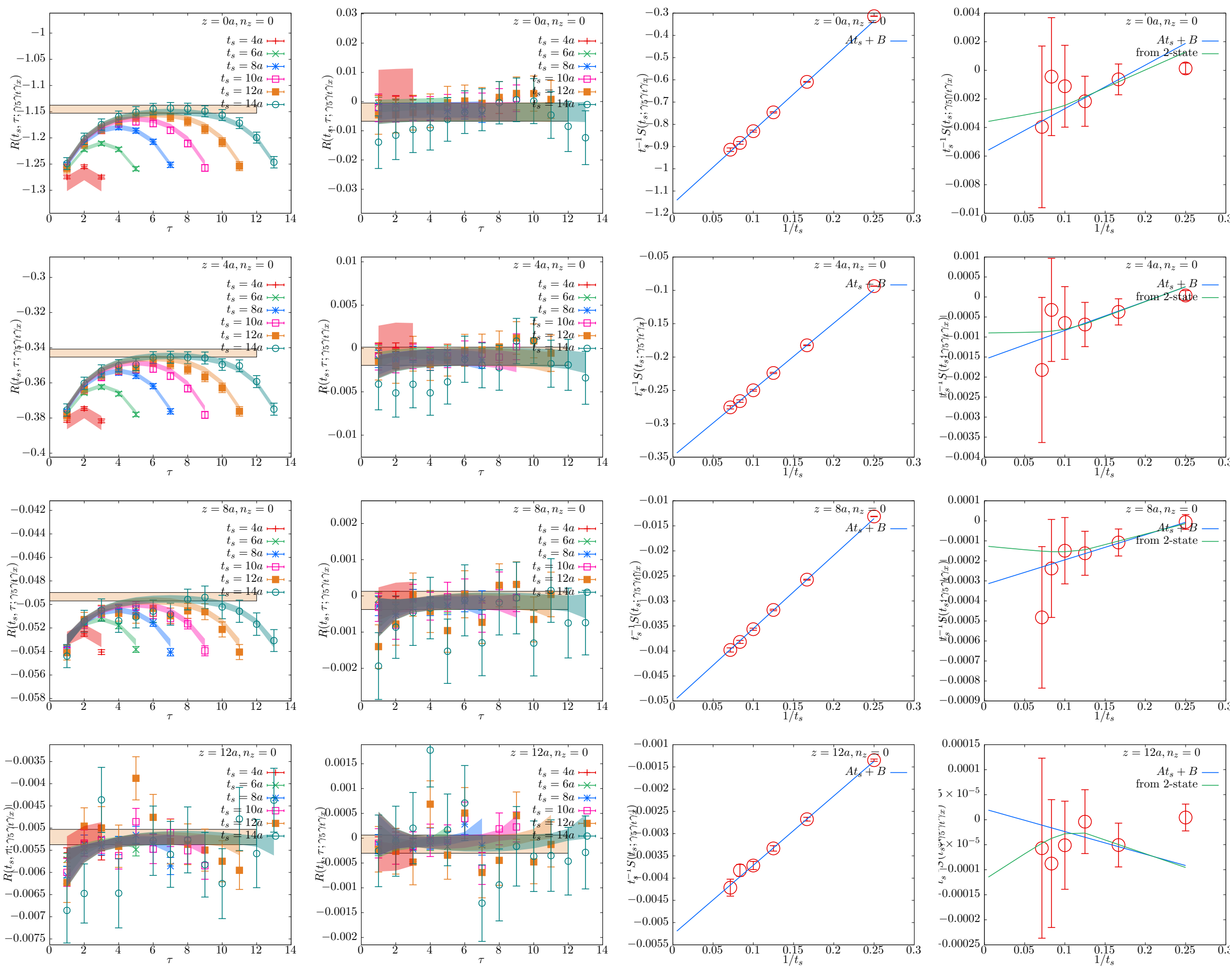

FIG. 20. 3pt analysis for $P_z = 0$ and $O_{\gamma_5\gamma_t\gamma_x}$. The different rows are analysis for specific values of z. Column-1 and 2 are for real and imaginary of ratio R as a function of operator insertion point τ. Diff colors are for diff t_s. The bands are fits using Fit(2,6,18,2). Column-3 and 4 are fits using summation methods to real and imag parts; what is shown is $S(t_s)/t_s$ as a function of $1/t_s$ which is expected to behave as $M_{00} + c/t_s$. The blue curve is the summation fit Sum(6,18,2). The green curve is the expected curve for $S(t_s)/t_s$ from 2-state fit method Fit(2,6,18,2).

Appendix A: Extrapolations to get the matrix elements

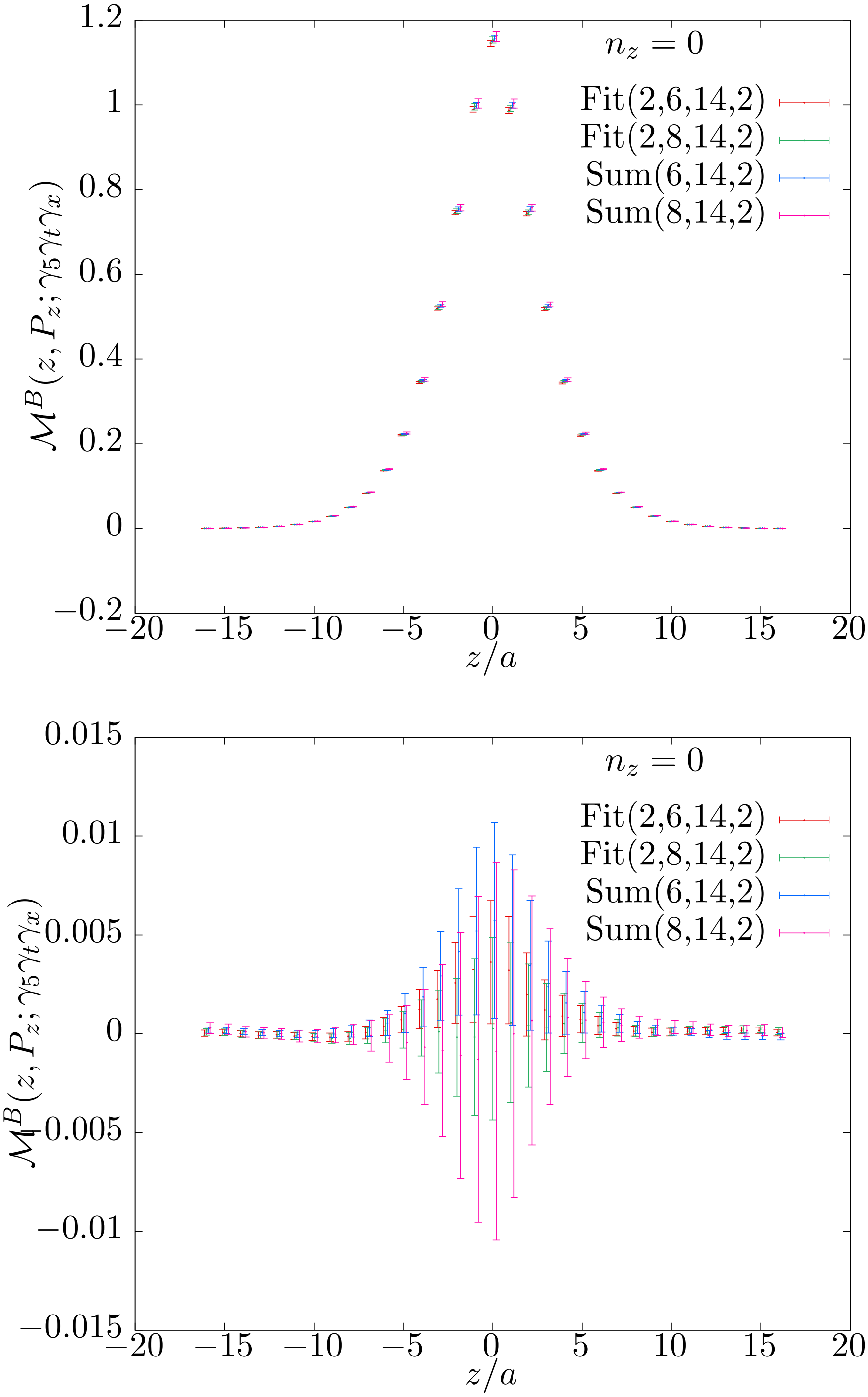

FIG. 21. Fit systematics for $P_z = 0$ and $\gamma_5\gamma_t\gamma_x$ matrix element; Re part on top, Im part in the bottom. For each z, results of extrapolated values of bare matrix elements M_{00} from different kinds of 2-state fit and summation fits are shown (and slightly displaced).

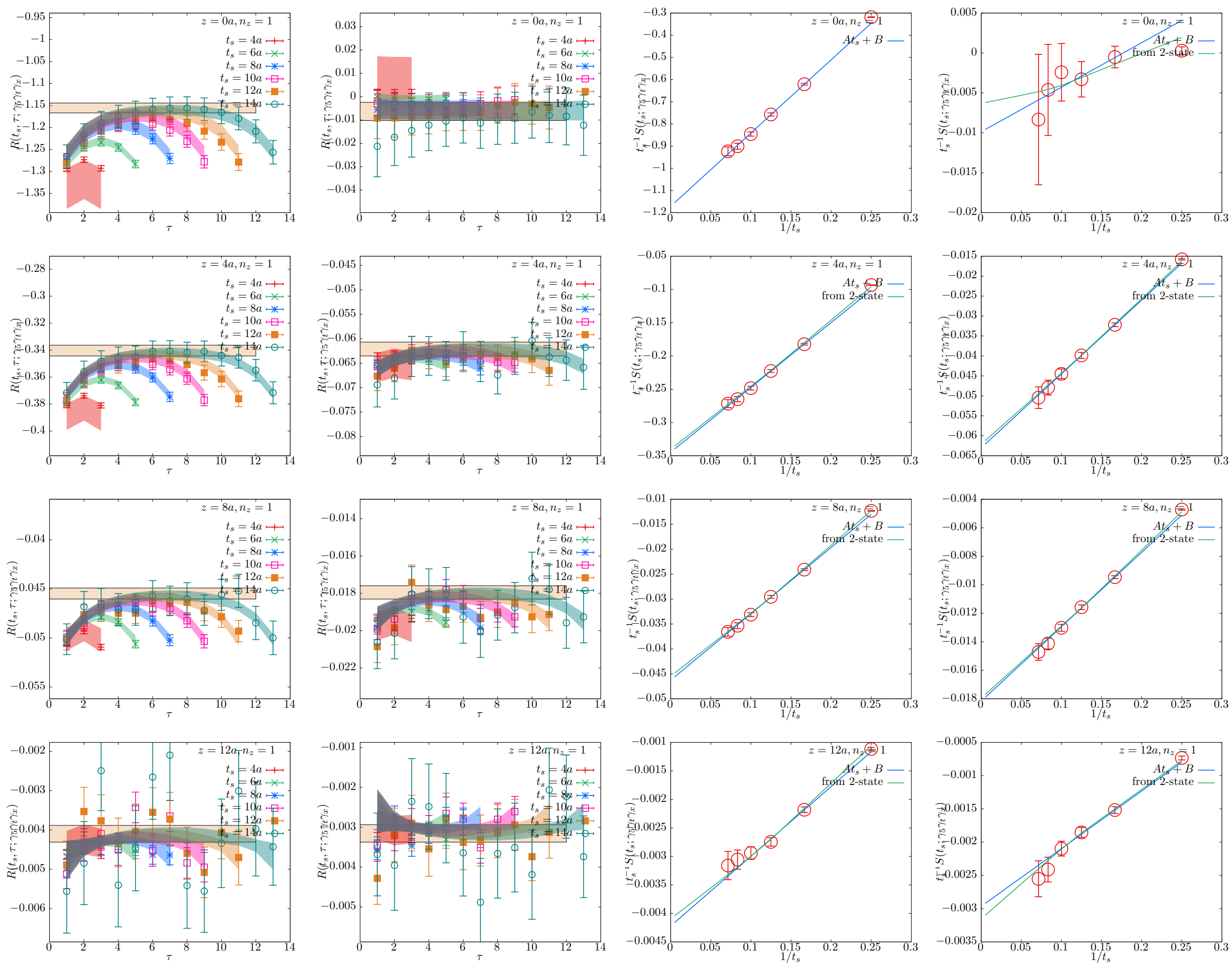

FIG. 22. 3pt analysis for $P_z = 1$ and $O_{\gamma_5\gamma_t\gamma_x}$. The different rows are analysis for specific values of z. Column-1 and 2 are for real and imaginary of ratio R as a function of operator insertion point τ. Diff colors are for diff t_s. The bands are fits using Fit(2,6,18,2). Column-3 and 4 are fits using summation methods to real and imag parts; what is shown is $S(t_s)/t_s$ as a function of $1/t_s$ which is expected to behave as $M_{00} + c/t_s$. The blue curve is the summation fit Sum(6,18,2). The green curve is the expected curve for $S(t_s)/t_s$ from 2-state fit method Fit(2,6,18,2).

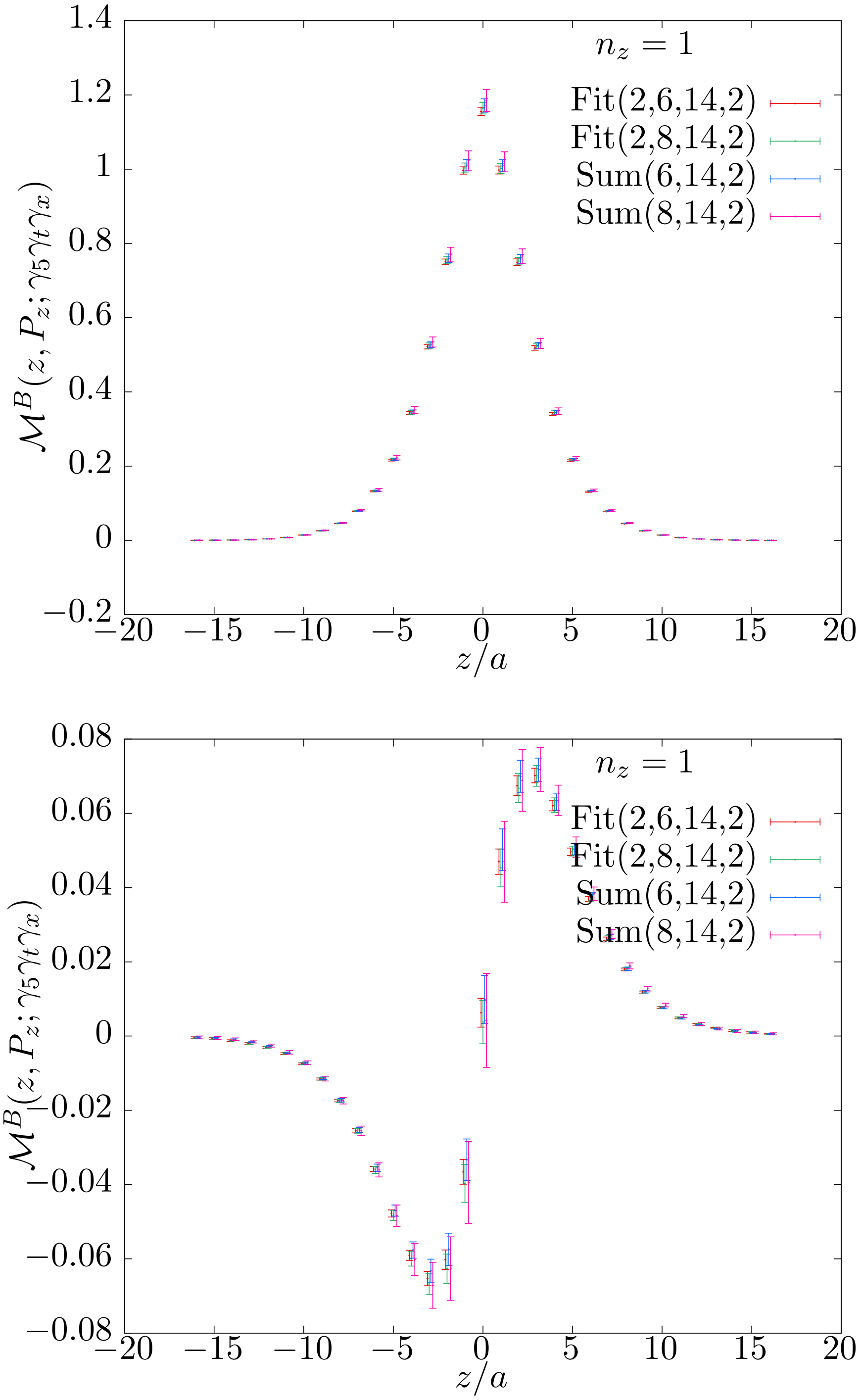

FIG. 23. Fit systematics for $P_z = 1$ and $\gamma_5\gamma_t\gamma_x$ matrix element; Re part on top, Im part in the bottom. For each z, results of extrapolated values of bare matrix elements M_{00} from different kinds of 2-state fit and summation fits are shown (and slightly displaced).

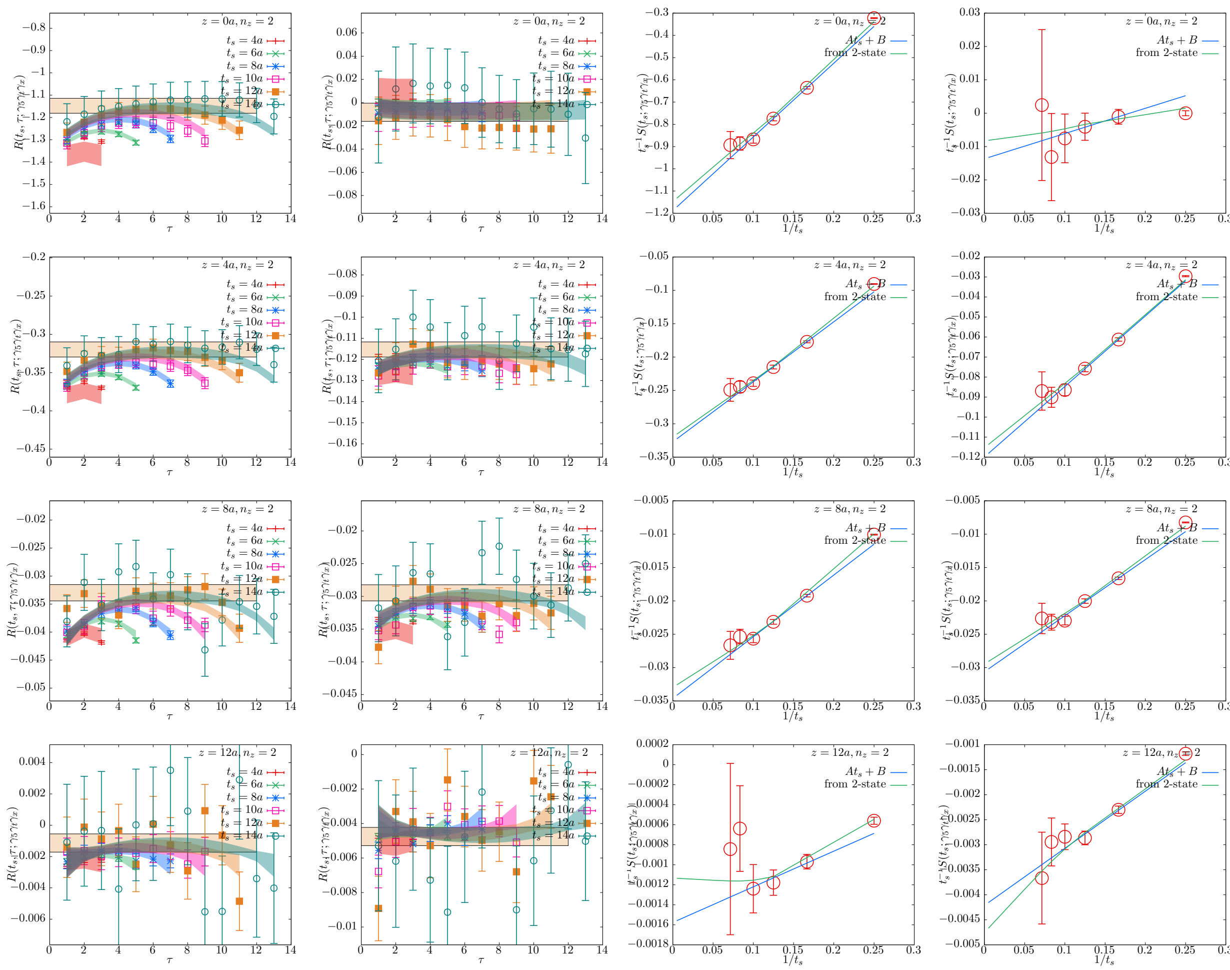

FIG. 24. 3pt analysis for $P_z = 2$ and $O_{\gamma_5\gamma_t\gamma_x}$. The different rows are analysis for specific values of z. Column-1 and 2 are for real and imaginary of ratio R as a function of operator insertion point τ. Diff colors are for diff t_s. The bands are fits using Fit(2,6,18,2). Column-3 and 4 are fits using summation methods to real and imag parts; what is shown is $S(t_s)/t_s$ as a function of $1/t_s$ which is expected to behave as $M_{00} + c/t_s$. The blue curve is the summation fit Sum(6,18,2). The green curve is the expected curve for $S(t_s)/t_s$ from 2-state fit method Fit(2,6,18,2).

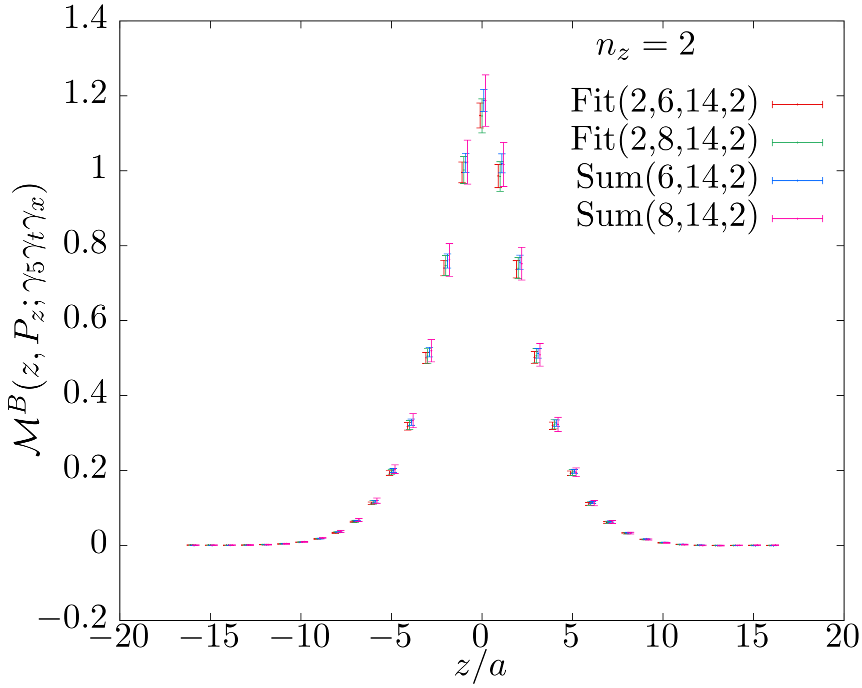

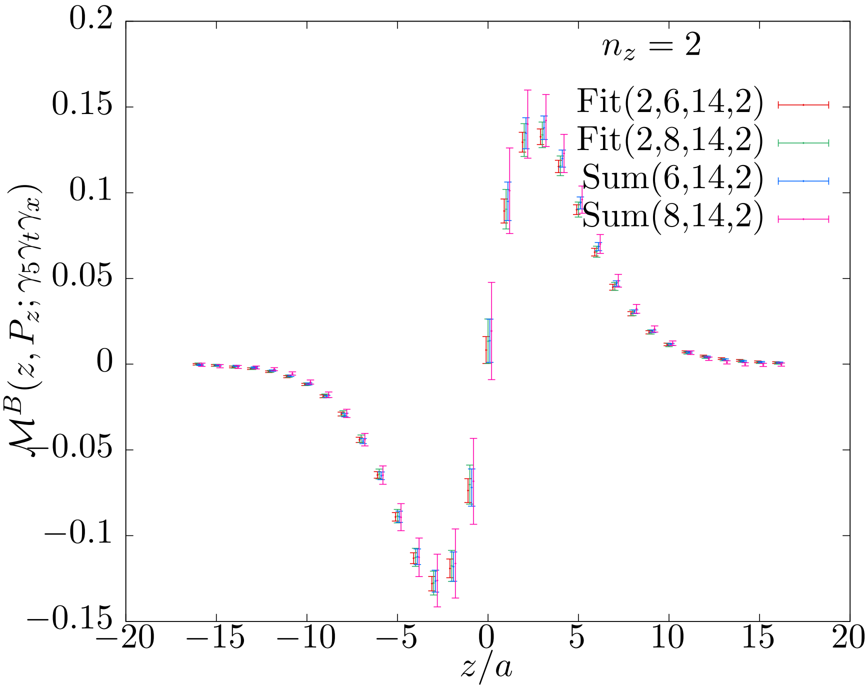

FIG. 25. Fit systematics for $P_z = 2$ and $\gamma_5\gamma_t\gamma_x$ matrix element; Re part on top, Im part in the bottom. For each z, results of extrapolated values of bare matrix elements M_{00} from different kinds of 2-state fit and summation fits are shown (and slightly displaced).

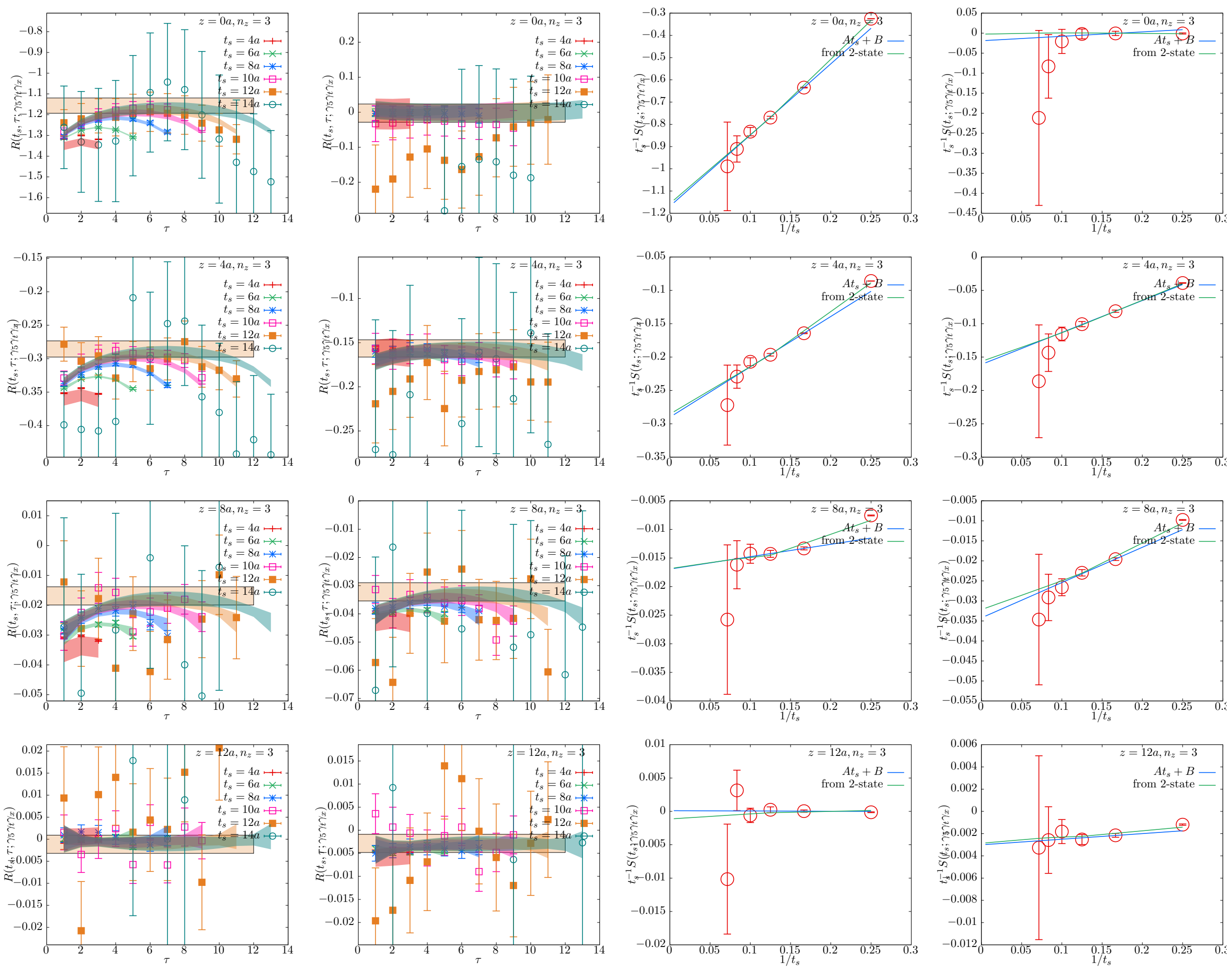

FIG. 26. 3pt analysis for $P_z = 3$ and $O_{\gamma_5\gamma_t\gamma_x}$. The different rows are analysis for specific values of z. Column-1 and 2 are for real and imaginary of ratio R as a function of operator insertion point τ. Diff colors are for diff t_s. The bands are fits using Fit(2,6,18,2). Column-3 and 4 are fits using summation methods to real and imag parts; what is shown is $S(t_s)/t_s$ as a function of $1/t_s$ which is expected to behave as $M_{00} + c/t_s$. The blue curve is the summation fit Sum(6,18,2). The green curve is the expected curve for $S(t_s)/t_s$ from 2-state fit method Fit(2,6,18,2).

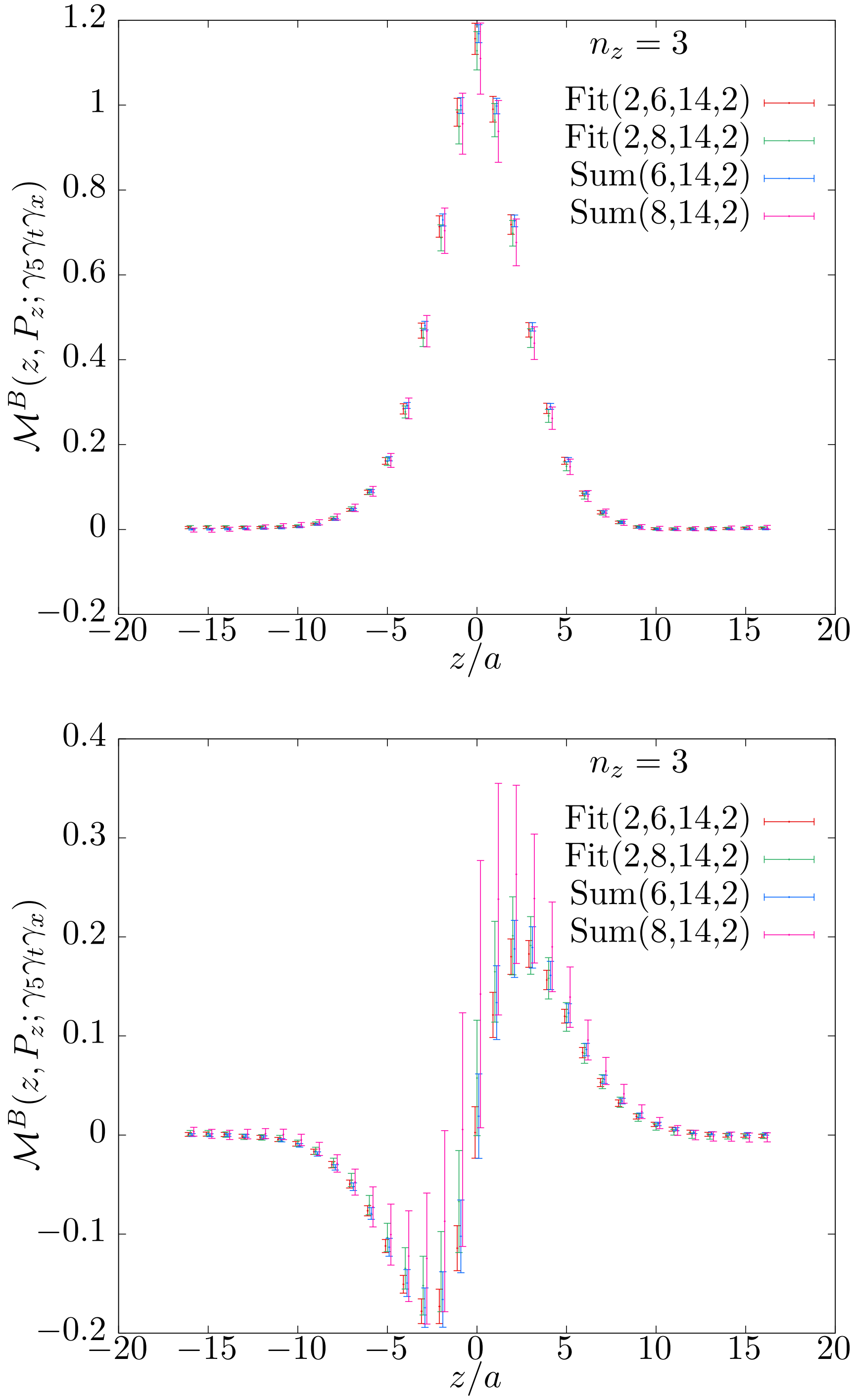

FIG. 27. Fit systematics for $P_z = 3$ and $\gamma_5\gamma_t\gamma_x$ matrix element; Re part on top, Im part in the bottom. For each z, results of extrapolated values of bare matrix elements M_{00} from different kinds of 2-state fit and summation fits are shown (and slightly displaced).

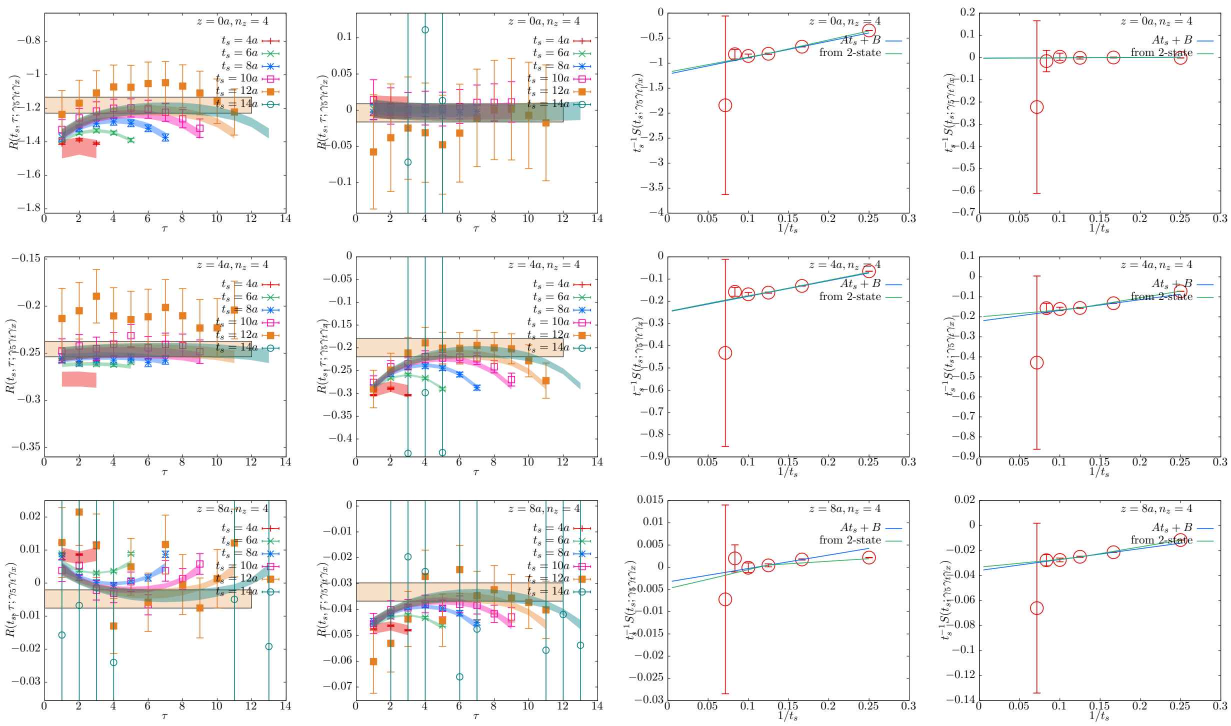

FIG. 28. 3pt analysis for $P_z = 4$ and $O_{\gamma_5\gamma_t\gamma_x}$. The different rows are analysis for specific values of z. Column-1 and 2 are for real and imaginary of ratio R as a function of operator insertion point τ. Diff colors are for diff t_s. The bands are fits using Fit(2,6,18,2). Column-3 and 4 are fits using summation methods to real and imag parts; what is shown is $S(t_s)/t_s$ as a function of $1/t_s$ which is expected to behave as $M_{00} + c/t_s$. The blue curve is the summation fit Sum(6,18,2). The green curve is the expected curve for $S(t_s)/t_s$ from 2-state fit method Fit(2,6,18,2).

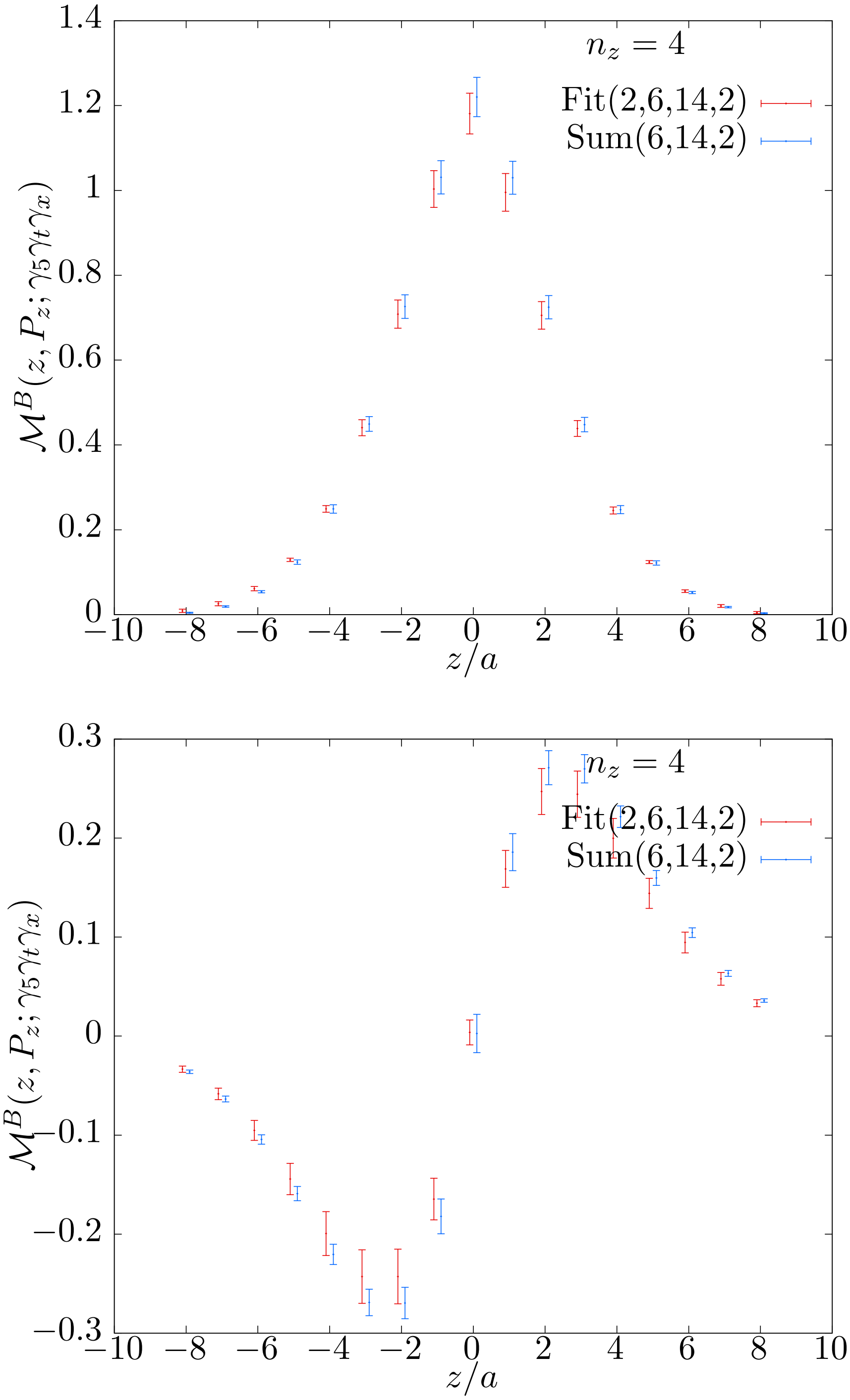

FIG. 29. Fit systematics for $P_z = 4$ and $\gamma_5\gamma_t\gamma_x$ matrix element; Re part on top, Im part in the bottom. For each z, results of extrapolated values of bare matrix elements M_{00} from different kinds of 2-state fit and summation fits are shown (and slightly displaced).

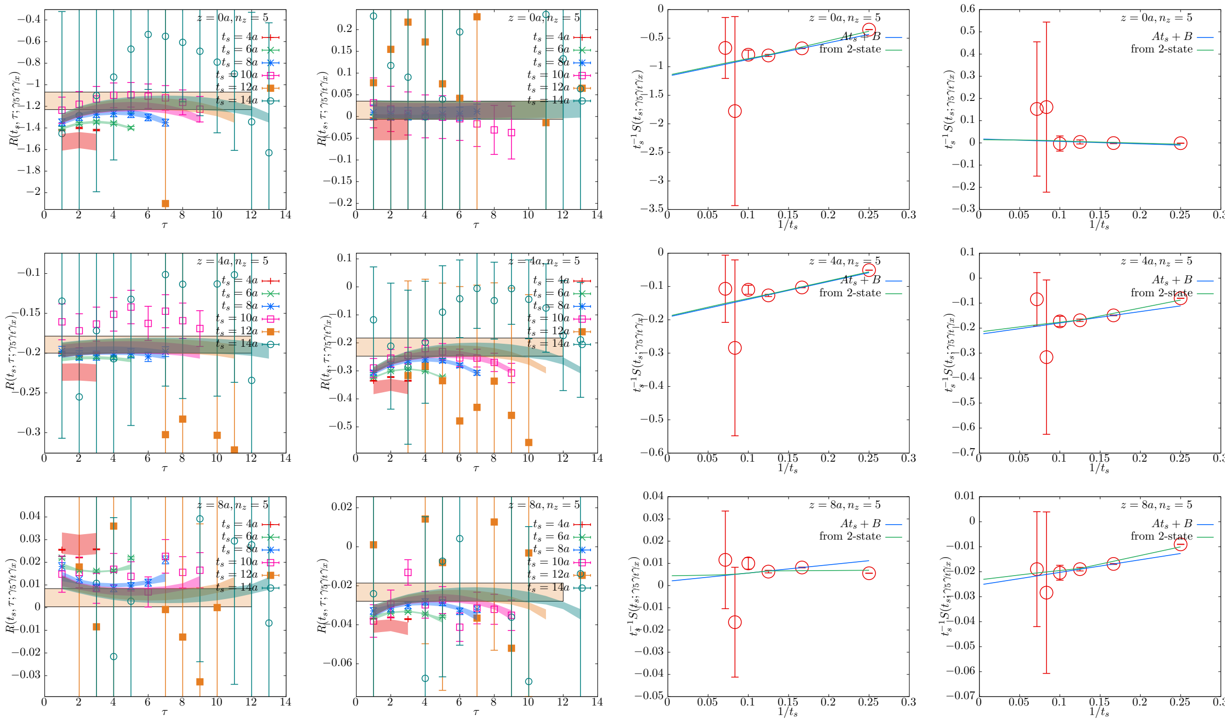

FIG. 30. 3pt analysis for $P_z = 5$ and $O_{\gamma_5\gamma_t\gamma_x}$. The different rows are analysis for specific values of z. Column-1 and 2 are for real and imaginary of ratio R as a function of operator insertion point τ. Diff colors are for diff t_s. The bands are fits using Fit(2,6,18,2). Column-3 and 4 are fits using summation methods to real and imag parts; what is shown is $S(t_s)/t_s$ as a function of $1/t_s$ which is expected to behave as $M_{00} + c/t_s$. The blue curve is the summation fit Sum(6,18,2). The green curve is the expected curve for $S(t_s)/t_s$ from 2-state fit method Fit(2,6,18,2).

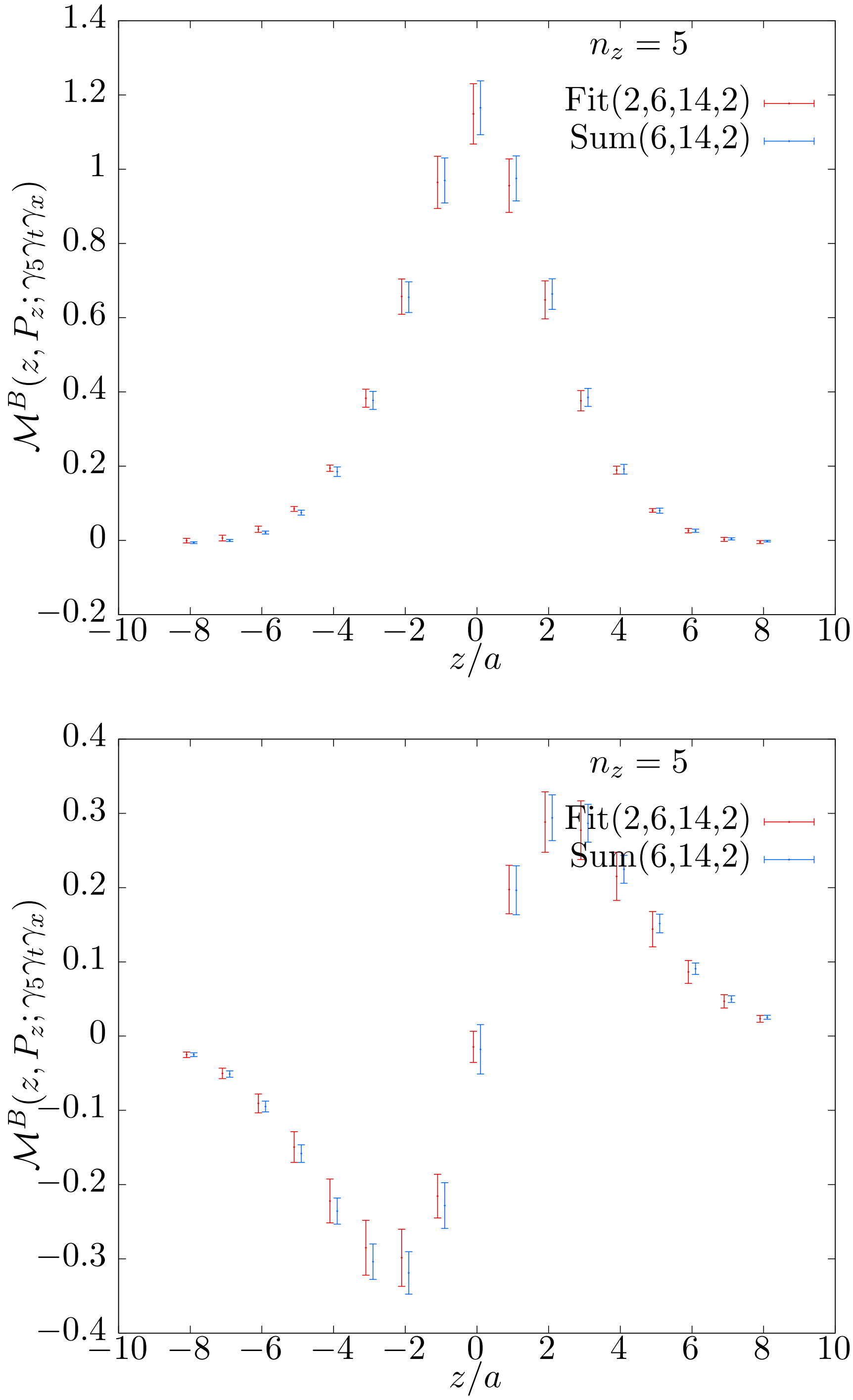

FIG. 31. Fit systematics for $P_z = 5$ and $\gamma_5\gamma_t\gamma_x$ matrix element; Re part on top, Im part in the bottom. For each z, results of extrapolated values of bare matrix elements M_{00} from different kinds of 2-state fit and summation fits are shown (and slightly displaced).

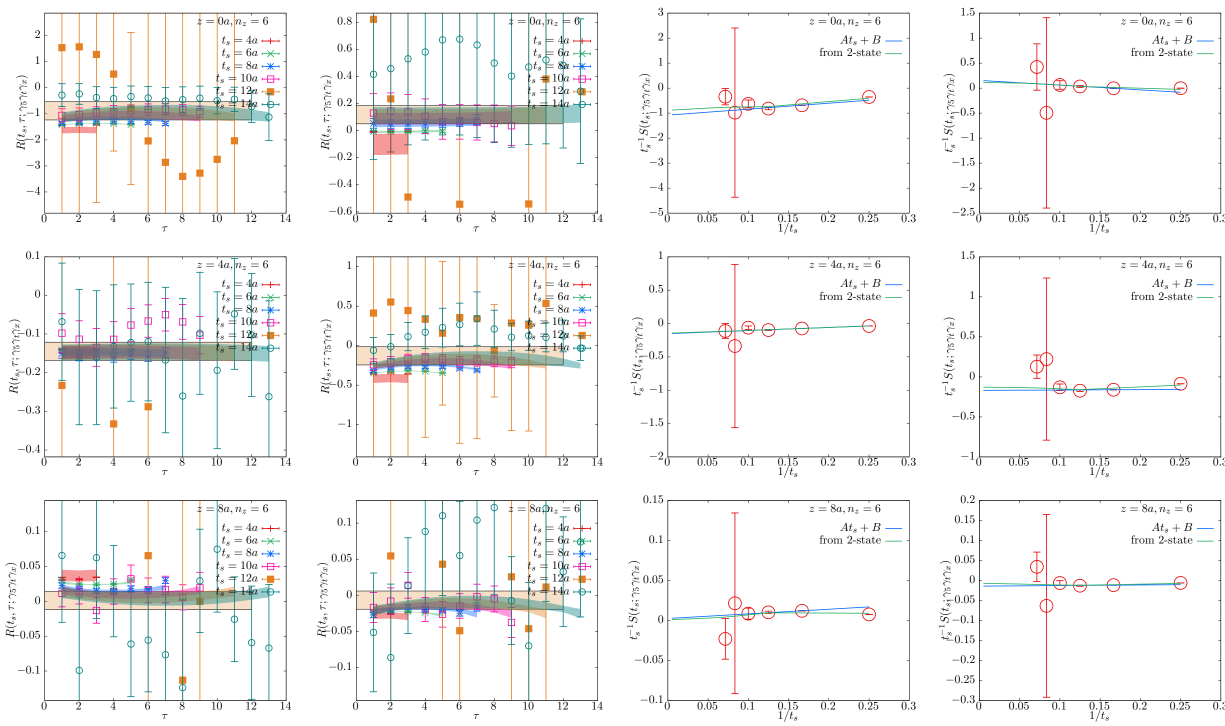

FIG. 32. 3pt analysis for $P_z = 6$ and $O_{\gamma_5\gamma_t\gamma_x}$. The different rows are analysis for specific values of z. Column-1 and 2 are for real and imaginary of ratio R as a function of operator insertion point τ. Diff colors are for diff t_s. The bands are fits using Fit(2,6,18,2). Column-3 and 4 are fits using summation methods to real and imag parts; what is shown is $S(t_s)/t_s$ as a function of $1/t_s$ which is expected to behave as $M_{00} + c/t_s$. The blue curve is the summation fit Sum(6,18,2). The green curve is the expected curve for $S(t_s)/t_s$ from 2-state fit method Fit(2,6,18,2).

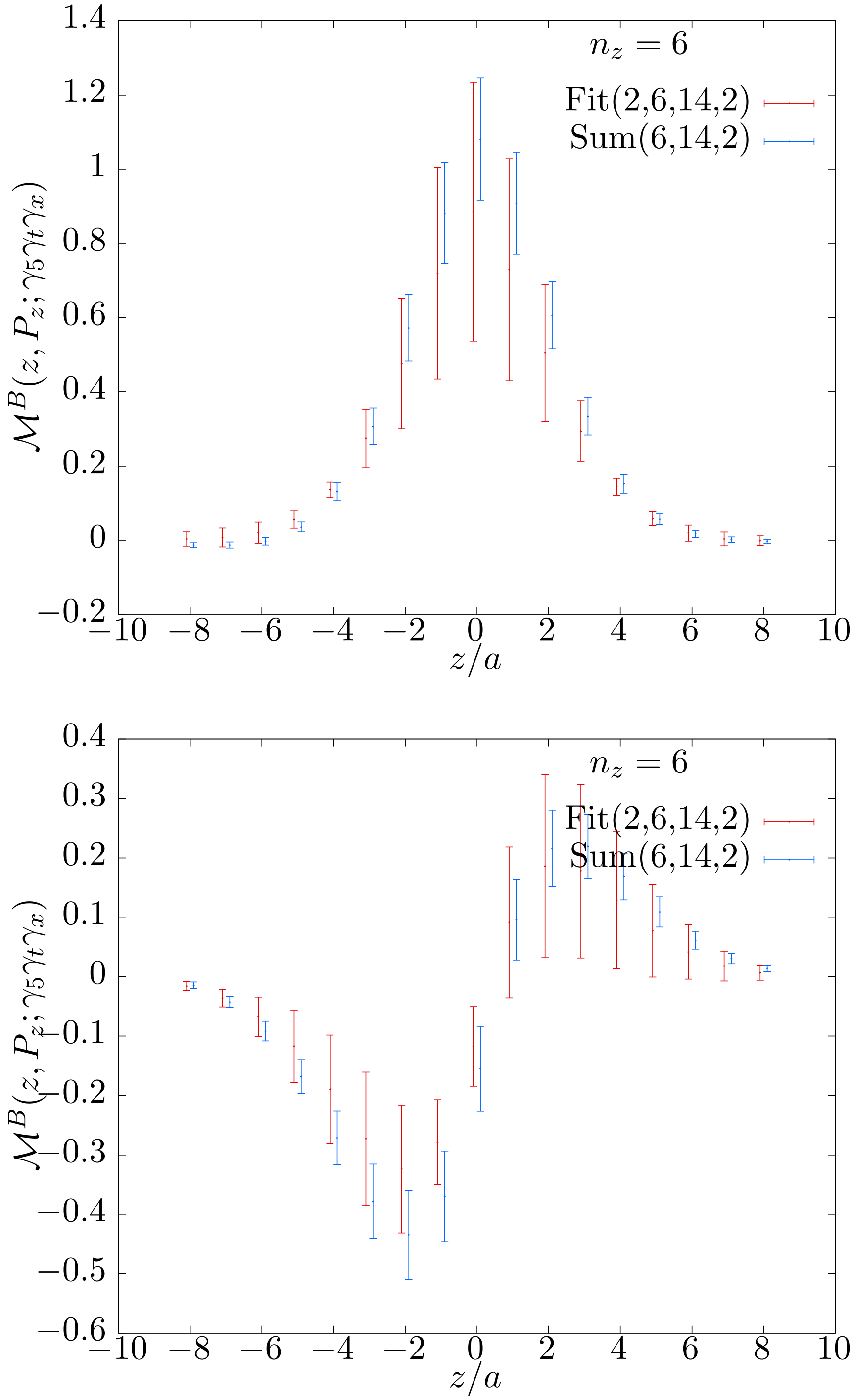

FIG. 33. Fit systematics for $P_z = 6$ and $\gamma_5\gamma_t\gamma_x$ matrix element; Re part on top, Im part in the bottom. For each z, results of extrapolated values of bare matrix elements M_{00} from different kinds of 2-state fit and summation fits are shown (and slightly displaced).

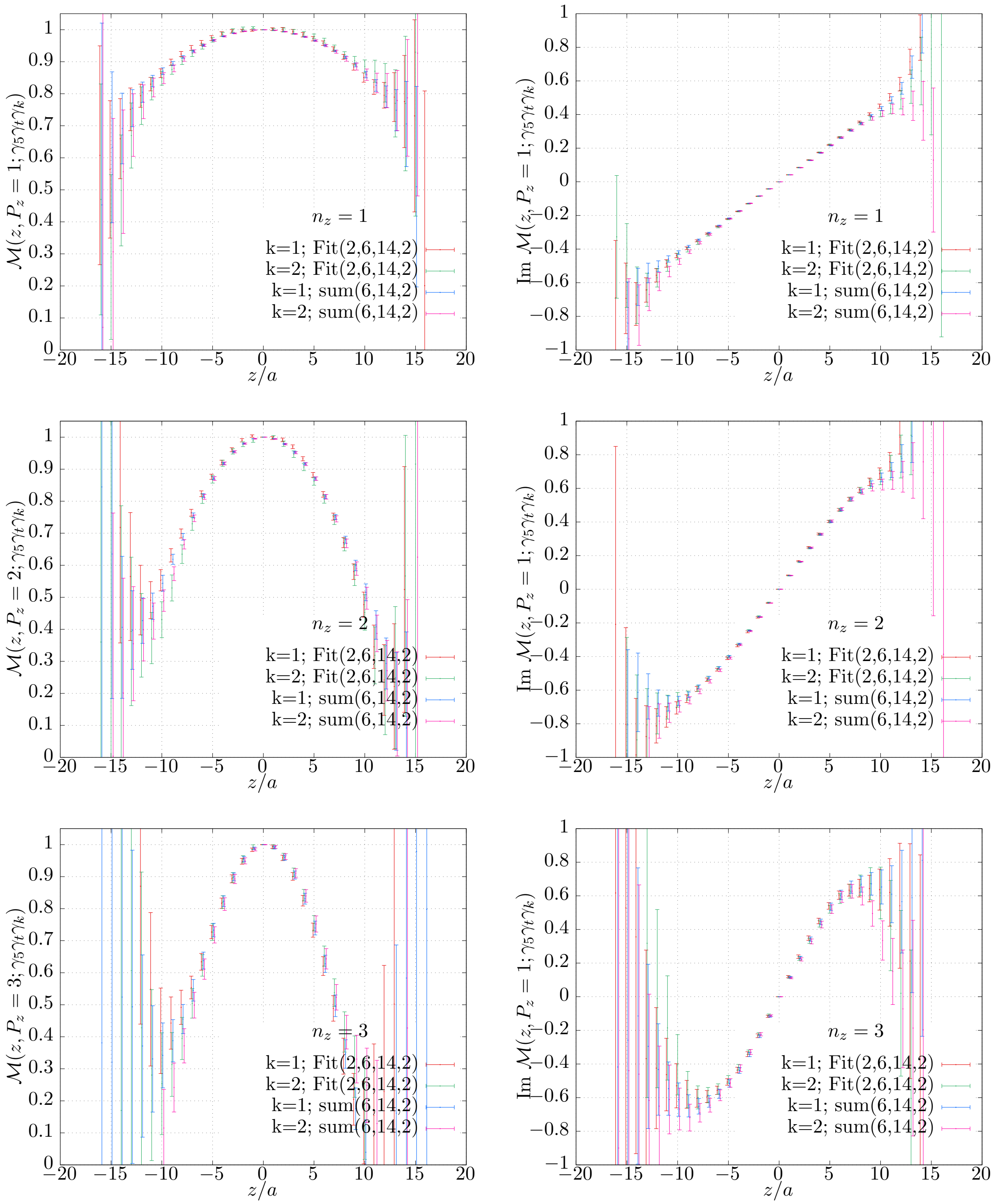

FIG. 34. ($P_z = 1, 2, 3$) Renormalized matrix element using "Choice-1" i.e., the operators $O_{\gamma_5\gamma_t\gamma_x}$ (k=1) and $O_{\gamma_5\gamma_t\gamma_y}$ (k=2) are treated separately. The results from fit (Fit(2,6,14,2)) and summation (Sum(6,14,2)) are compared. The results at $+|z|$ and $-|z|$ have not been symmetrized or anti-symmetrized in the data. The summation method leads to more precise values of $\mathcal{M}$ after taking double ratio in spite of errors in summation method being larger than in 2-state fits before taking the double ratio; the reason being that the correlation between different shorted z being larger for summation than for fit.

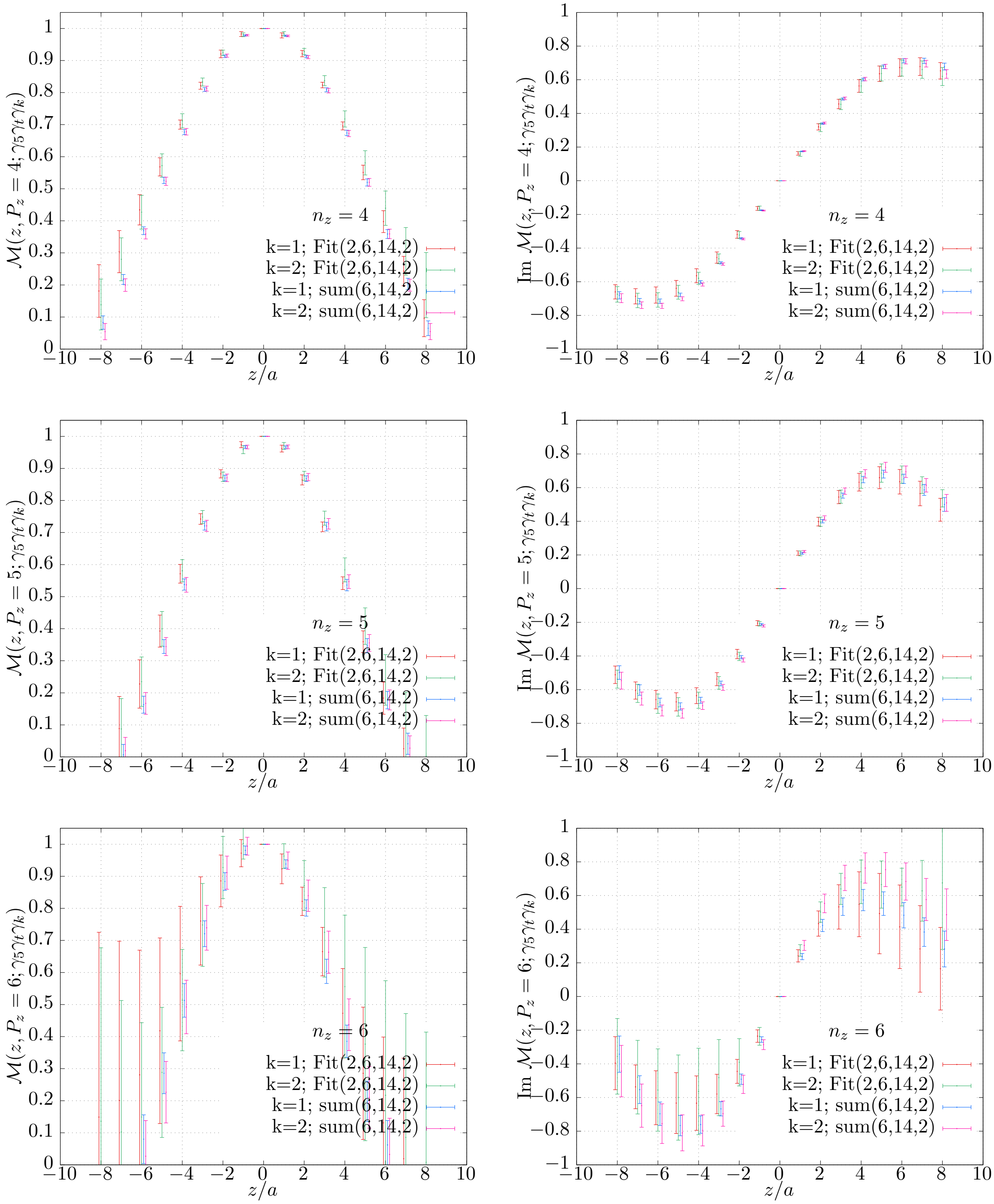

FIG. 35. ($P_z = 4, 5, 6$) Renormalized matrix element using "Choice-1" i.e., the operators $O_{\gamma_5\gamma_t\gamma_x}$ (k=1) and $O_{\gamma_5\gamma_t\gamma_y}$ (k=2) are treated separately. The results from fit (Fit(2,6,14,2)) and summation (Sum(6,14,2)) are compared. The results at $+|z|$ and $-|z|$ have not been symmetrized or anti-symmetrized in the data. The summation method leads to more precise values of $\mathcal{M}$ after taking double ratio in spite of errors in summation method being larger than in 2-state fits before taking the double ratio; the reason being that the correlation between different shorted z being larger for summation than for fit.

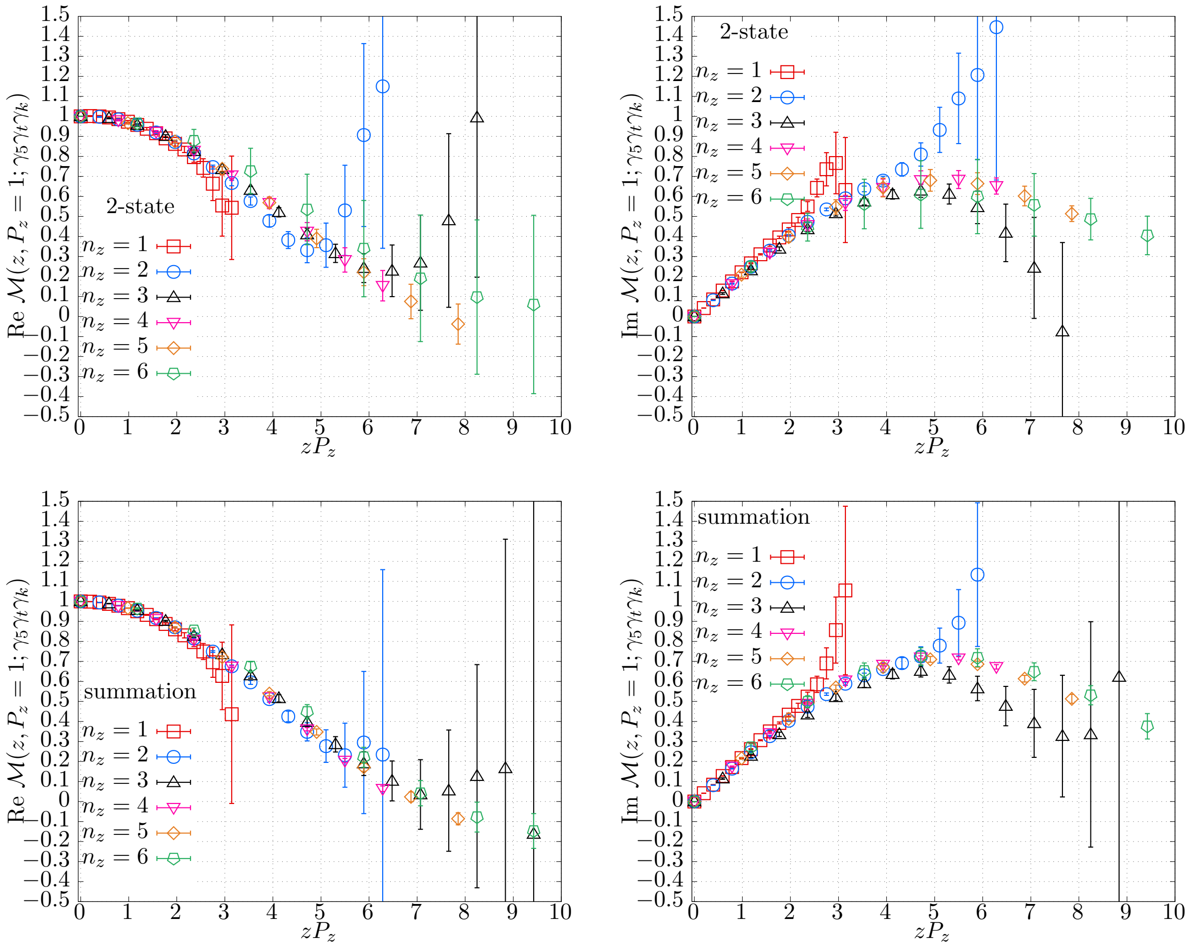

FIG. 36. The renormalized ITD (using "Choice-2") has been shown as a function of $\nu = zP_z$. The real and imag parts are on the left and right. The results using 2-state and summation method on top and bottom panels. The results for ITD at fixed P_z are differentiated by color, and all z at each P_z have been shown.